J. Fluid Mech. (1993), *vol.* 249, *pp.* 619–664

The instability and breakdown of a round variable-density jet

By D. M. KYLE AND K. R. SREENIVASAN
Department of Mechanical Engineering, Mason Laboratory, Yale University, New Haven, CT 06520, USA

(Received 23 May 1991 and in revised form 10 November 1992)

A study has been made of the instability and the subsequent breakdown of axisymmetric jets of helium/air mixtures emerging into ambient air. Although the density of the nozzle gas is less than that of the ambient fluid, the jet is essentially non-buoyant. Two kinds of instability are observed in the near field, depending upon the mean flow parameters. When the ratio of the exiting nozzle fluid density to ambient fluid density is $\rho_e/\rho_\infty > 0.6$, shear-layer fluctuations evolve in a fashion similar to that observed in constant-density jets: the power spectrum near the nozzle is determined by weak background disturbances whose subsequent spatial amplification agrees closely with the spatial stability theory. When the density ratio is less than 0.6, an intense oscillatory instability may also arise. The overall behaviour of this latter mode (to be called the 'oscillating' mode) is shown to depend solely upon the density ratio and upon D/θ, where D is the nozzle diameter and θ is the momentum thickness of the boundary layer at the nozzle exit. The behaviour of this mode is found to be independent of the Reynolds number, within the range covered by the present experiments. This is even true in the immediate vicinity of the nozzle where, unlike in the case of shear-layer modes, the intensity of the oscillating mode is independent of background disturbances. The streamwise growth rate associated with the oscillating mode is not abnormally large, however. The frequency of the oscillating mode compares well with predictions based on a spatio-temporal theory, but not with those of the standard spatial theory.

From high-speed films it is found that the overall structure of the oscillating mode repeats itself with extreme regularity. The high degree of repeatability of the oscillating mode, in association with a strong pairing process, leads to abnormally large centreline velocity fluctuation, with its root-mean-square value being about 30% of the nozzle exit velocity. Energetic and highly regular pairing is found also to lead to the early and abrupt breakdown of the potential core. The regularity often extends even to the finer structure immediately downstream of the breakdown. An attempt is made to explain these special features both in terms of the large-amplitude vorticity field, and in terms of the theoretically predicted space–time evolution of wave packets.

1. Introduction

Except at very low Reynolds numbers, a laminar shear layer with constant density is unstable to arbitrarily small disturbances. These disturbances evolve by selective amplification as they convect downstream (Cohen & Wygnanski 1987). The migration of vorticity resulting from the instability forms axisymmetric or helical structures accompanied by large-amplitude fluctuations. Generally, these structures interact with one another and contribute significantly to entrainment and mixing by convective

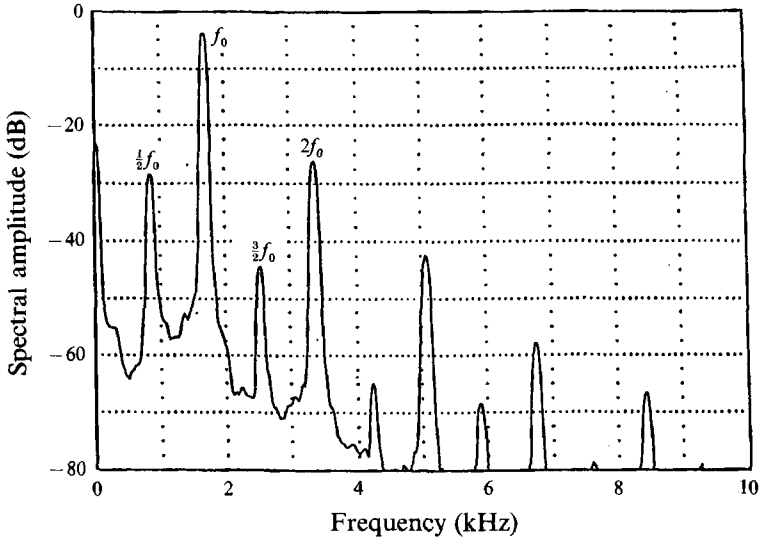

FIGURE 1. Power spectral density in a helium jet ($S = 0.14$), showing large peaks at f_0, its subharmonic, $\frac{1}{2}f_0$, and several harmonics. The hot wire was located along the jet centreline at 1.33 diameters downstream of the nozzle exit. The frequency f_0 of the oscillating mode does not depend on the spatial position in that region. (Taken from Sreenivasan *et al.* 1989.)

transport (Winant & Browand 1974), and to the generation of acoustic noise (Crighton 1975; Sarohia & Massier 1977; Kibens 1980). Very often, engineering interest arises when the nozzle fluid density ρ_e is significantly less than the ambient fluid density, ρ_∞. The kinematics and dynamics in the near field of variable density jets is the focus of the present study. Before discussing its specific objectives, it is helpful to review the previous literature on the subject. This is best done by reviewing the experimental and theoretical studies separately.

1.1. *Experiment*

Several early studies indicate that the mean flow evolution in the near field can be sensitively dependent upon the density ratio, $S = \rho_e/\rho_\infty$. Corrsin & Uberoi (1949) measured the temperature and velocity fields for various nozzle gas temperatures in heated air jets. For temperatures corresponding with $S = 0.95$ and 0.62, they found that the potential core terminated at $x/D \approx 5$, where x is the distance along the axis and D is the nozzle orifice diameter. When S was decreased to 0.49, however, the potential core terminated at $x/D \approx 3.5$, followed by a relatively sharp drop in the centreline temperature and velocity. Beyond the potential core, the jet width for $S = 0.49$ was approximately twice that for $S = 0.95$. Data obtained by Landis & Shapiro (1951) and Sforza & Mons (1978) in heated air jets, and by Chriss (1968), Tombach (1969) and by Abramovich *et al.* (1969) in heterogeneous jets confirm that, below $S \approx 0.60$, mixing processes are significantly enhanced in the near field. Abramovich *et al.* (1969) measured the spread rate of the shear layer and found that in addition to the dependence on the density ratio, spread rates were also sensitively dependent upon the jet Reynolds number and upon the initial shear-layer thickness.

There is evidence to suggest that the mean flow variations described above may be linked to abnormally intense instability modes sustained only when the density ratios are small. Smith & Johannesen (1986) obtained power spectra using microphones located in the acoustic far field of helium/argon jets issuing into air. In pure helium jets

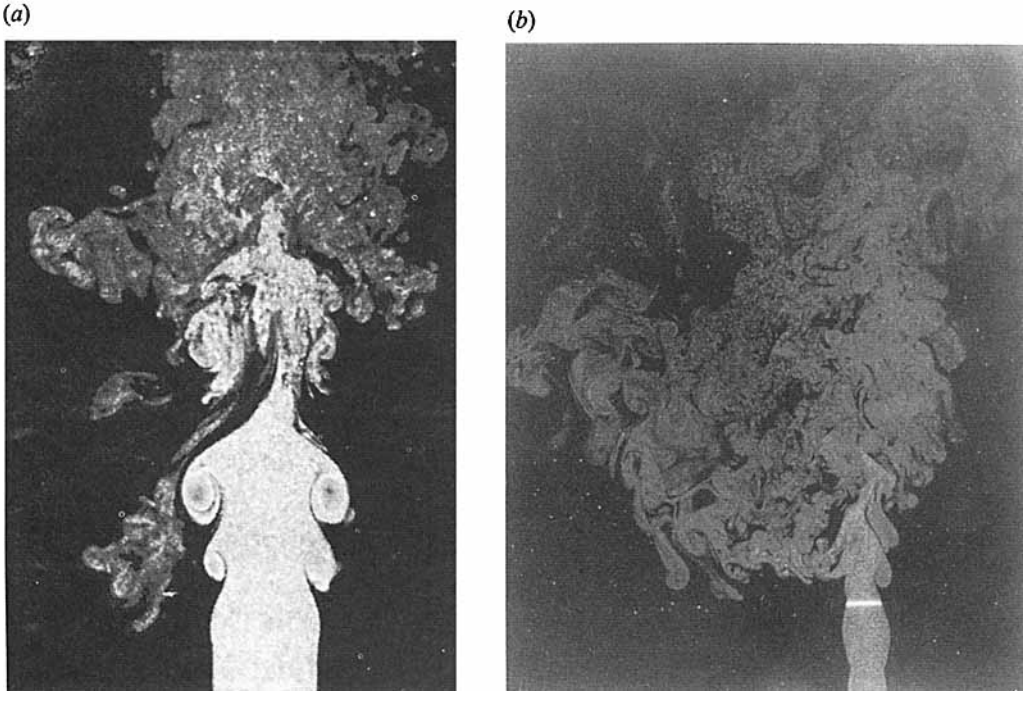

FIGURE 2. (*a*) Instantaneous digital image of the aerosol distribution in the axial plane of a seeded flow. A single pulse from a YAG laser illuminates the flow. $S = 0.29$. (Taken from Kyle 1988.) (*b*) A typical realization of the helium jet issuing from the nozzle into ambient air; the jet spreads very rapidly beyond a reasonably well-defined streamwise position. The figure is taken from Sreenivasan *et al.* (1989), where details are given of how this picture was obtained; see also §2 of the text. $Re = 1400$, $S = 0.14$, nozzle diameter = 6 mm.

they discovered an oscillatory jet instability for Mach numbers below 0.56. Reminiscent of the mean flow results of Abramovich *et al.* (1969), this instability was found to depend upon the precise nozzle contour. The density dependence of jet noise for higher velocities is reported by Hoch *et al.* (1973) and by Chan & Leong (1973). Kyle (1986) and Sreenivasan, Raghu & Kyle (1989) examined spectra obtained along the centreline of low-speed helium/air jets, and found that the jet instability of the type observed by Smith & Johannesen is sustained in jets with density ratios at least as large as 0.5. These authors showed that the oscillatory behaviour can dominate the flow in the entire near field (see figure 1). Monkewitz *et al.* (1990) have obtained similar results in heated air jets.

The observation that the spectral density function is dominated by a discrete frequency spike of large magnitude and its higher harmonics, quite unlike the situation in constant density jets, suggests the occurrence of a new phenomenon. The time records used for calculating these spectra are so long that many wave crests pass by the fixed hot-wire position during a single time record. In order to produce such 'spiky' spectra, there must be relatively little random variation from one passing structure to the next, or the modes must preserve their phase over many cycles. Stationary images in the near field of variable-density jets reveal that the spiky power spectra are indeed accompanied by extremely coherent ring vortices formed along the jet column, as exemplified by figure 2(*a*) and other photographs presented by Kyle (1988), Sreenivasan *et al.* (1989) and Monkewitz *et al.* (1989). We shall denote this henceforth as the 'oscillating mode'. Radial profiles of the mean temperature (Monkewitz *et al.* 1990)

suggest that these structures may be unusually effective in convective transport. The variable-density jet can undergo a catastrophic spread near the end of the potential core, as seen in figure 2(*b*) (see also Sreenivasan *et al.* 1989; Monkewitz *et al.* 1989). This spread is associated with the radial ejection of fluid in the form of 'side jets' (Monkewitz *et al.* 1989), which may be due to the growth of azimuthal instabilities in the highly strained region between the vortex rings (Liepmann 1991). At the end of the potential core, the ring structures vanish (figure 2). Power spectra generally show that the subharmonic reaches its maximum towards the end of the potential core (Kyle 1986, 1988), suggesting the occurrence of vortex pairing (Ho & Huang 1982).

In addition to variable-density jets, several other flows such as wakes (e.g. Strykowski & Sreenivasan 1990) and countercurrent shear layers (e.g. Strykowski & Niccum 1992) show similarly well-ordered structure under certain conditions. Partly in an effort to explain these observations, the theoretical framework of space–time instability of fluid flows has seen a resurgence in the last few years. Since we wish to remark on the applicability of the theory to our experiments, it is necessary to review the theory briefly.

1.2. *Theory*

Even though the organized state that we are trying to explain here is highly nonlinear, the theory – which purports to explain the onset of this state – is linear. Unlike temporal instability of the basic state where one considers the growth in time of spatially periodic perturbations, or the spatial instability where one considers the steady-state response of the basic state to spatially localized but time-periodic disturbances, it has been found more useful to study the response of a quiescent system for $t < 0$, perturbed impulsively by a disturbance of the form $\sim \delta(x)\,\delta(t)$. The resulting disturbance takes the form of a wave packet, as discussed by Sturrock (1958), Briggs (1964), Gaster (1968*a*, *b*) and Huerre & Monkewitz (1985), among others. The wave packet may be regarded as the Green function from which the complete response to any distributed perturbation can be deduced.

Using closely related formulations, Briggs (1964) and Gaster (1968*a*, *b*) have shown that if the wave packet evolves over a long period of time, then the motion at every point (x, t) in the physical plane which results from a single pulse perturbation can be associated with a specific wavenumber k. Thus for quite general conditions (Bers 1983), along each trajectory $x/t =$ constant the fluid motion is eventually dominated by a single complex wavenumber k^*, which simultaneously must satisfy the two relations:

$$\partial\omega_{\mathrm{i}}(k^*)/\partial k_{\mathrm{r}} = 0, \tag{1.1}$$

$$\partial\omega_{\mathrm{r}}(k^*)/\partial k_{\mathrm{r}} = x/t. \tag{1.2}$$

We may view (1.1) and (1.2) as determining $k^*(x/t)$ for any given x/t. Note that the functions ω_{r}, ω_{i} are just the real and imaginary components of the dispersion relation.

Our intention is not to review the mathematics which leads to (1.1) and (1.2), but to point out its physical content to the extent needed here. Each wave excited by the impulse perturbation immediately starts to grow (or attenuate) and propagate at a distinct, finite rate. In due course, the energy associated with certain of these modes will tend to prevail in particular locations. To see which modes prevail and at what locations, let us imagine several observers of this system, each moving at a different speed x/t. At first, each observer may notice many of the excited waves that are propagating at his speed, but one wave will eventually dominate his field of view; it is the wave which simultaneously has an associated real group velocity that matches the observer's speed (equation (1.2)), and has a transient growth rate ω_{i} that is a maximum

in the sense of (1.1). If several wavenumbers $k^*(x/t)$ satisfy (1.1) and (1.2), the one which has the largest growth rate will dominate. Because there is only a single dominant mode at large time for each x/t, the disturbance will appear to each observer as a discrete frequency wavetrain having wavelength $k_r^*(x/t)$ and frequency $\omega_r(k^*)$, and will appear to grow in space and time as $\sim \exp[-(k_i^*(x/t))x + \omega_i(k^*)\,t]$.

In certain systems, the wave packet will evolve in such a way that the observer moving with speed $x/t = 0$ will see the mode with wavenumber $k^*(0)$ grow with time, i.e. that $\omega_i(k^*(0)) > 0$. As pointed out earlier, this mode alone will eventually dominate the observer's field of view. This behaviour has been analysed explicitly by Gaster (1968*a*), Briggs (1964) and others (see the review by Huerre & Monkewitz 1990), and is called 'absolute instability'. It has further been shown that when $\omega_i(k^*(0)) > 0$, discrete frequency oscillations will evolve near the origin not only in response to an impulse perturbation, but also in response to nearly any spatially localized perturbation with arbitrary time dependence (see Briggs 1964, §2.3.5). Often in real flows, natural excitation resembles a continual random process that is localized in space (e.g. at the system boundary). It is therefore compelling to conjecture that if such a flow resembles in some approximate sense an absolutely unstable system, it may support oscillatory instabilities of the sort described earlier.

Gaster & Davey (1968) have examined the wavepacket which evolves from an impulse perturbation in the inviscid wake. In this study, $k^*(x/t)$ and $\omega(k^*)$ were calculated for a range of x/t. The particular wake profiles which they examined were not absolutely unstable. Huerre & Monkewitz (1985) have evaluated the impulse response in a plane shear layer between two parallel streams, and found for certain countercurrent flows that $\omega_i(k^*(0)) > 0$, i.e., if perturbed locally, this idealized system will eventually develop oscillations with frequency $\omega_r(k^*(0))$ at fixed points surrounding the space–time origin. Koch (1985) has examined the wake for a broad range of profiles and found that the wake can also be absolutely unstable. Pavithran & Redekopp (1989) have studied the impulse response for variable-density shear layers, while Monkewitz & Sohn (1986, 1988) have examined heated round jets. These latter authors found for a family of density and velocity profiles that the jet is absolutely unstable when S is sufficiently small.

1.3. *Motivation for the present work and the organization of the paper*

This experimental investigation is aimed at obtaining a clearer physical understanding of unstable modes which evolve in the near field (or the transition region) of variable-density jets. A key feature of these experiments is that they are well controlled, in that they explore – within the ranges covered – the dependence of the flow on each of the important governing parameters separately, while the others are fixed. We have chosen conditions for which the flow is incompressible and buoyancy effects are negligible.

We had earlier (Kyle 1986; Sreenivasan *et al.* 1989) performed an experimental investigation of the S-dependence of the oscillatory mode, and found that at some jet speeds, the measured onset value of S roughly corresponded with the theoretical value for which $\omega_i(k^*(0))$ first became positive. Monkewitz *et al.* (1990) found this behaviour in heated jets as well, and further observed that the Strouhal number generally falls within the range predicted by their theory. Detailed quantitative comparisons between theory and observation for corresponding values of governing parameter values have not been made, primarily because of the lack of experimental control already discussed. An added motivation for the present study is to compare, where possible for a relatively wide parameter range, the predicted parametric dependence of the onset of the instability with the observed behaviour.

The rest of the paper is organized as follows. After a discussion in §2 of the experimental conditions, we discuss in §3 the parameters governing the jet behaviour near the onset of oscillating mode and argue that it should depend essentially upon the Reynolds number, the density ratio, the ratio of nozzle diameter to shear-layer thickness, and background disturbances. In §4, we discuss measurements focusing on obtaining a time-resolved kinematic description of the oscillating mode and its subsequent breakdown process; using a set of high-speed films obtained for a range of parameter values, in conjunction with laser Doppler velocimetry measurements, we study the growth and interaction of large-amplitude waves associated with both the oscillating mode and normal shear layer modes. In §5, we concentrate on features of the power spectrum obtained in the region close to the nozzle exit, where the disturbances are small; we study the intensity and the frequency of each kind of mode as functions of the four governing parameters and of the streamwise distance. Emphasis is placed on the behaviour of the oscillating mode near onset, and on distinguishing the different kinds of instability existing in variable-density jets. Where appropriate, comparisons between experiment and theory are noted. As an aid to understanding the origin of the oscillating mode, we discuss in §6 its response to acoustic forcing and other changes in the environment. The paper concludes with §7 in which the nature of the oscillating mode is discussed in terms of both vorticity and the space–time instability. The Appendix summarizes certain issues involved in interpreting the hot-wire measurements made in the inhomogeneous flow considered here.

2. Experimental arrangement

The jet facility consists of a stainless steel settling chamber with screens of varying gradation and a capability for attaching matching nozzles of different exit diameters. The nozzle and the settling chamber are movable while the optical table surrounding the nozzle is fixed, making measurements at various streamwise locations relatively easy. Details of the facility are described in Stein (1969). Measurements were made with nozzles of 9.3 and 13.3 mm, both machined from aluminium stock. The 9.3 mm nozzle (contraction ratio 190) is designed using a cubic equation for the contour (Hussain & Ramjee 1976), and the 13.3 mm nozzle (contraction ratio 93) is designed with an ASME series low β contour (Bean 1971).

Various densities of the jet fluid were obtained by mixing helium and air in desired proportions. Before being mixed, the helium and air flow rates were metered separately using calibrated rotameters. The calibrations were carried out separately by correlating the rotameter readings with the volumetric discharge Q through the nozzle. Q was calculated using

$$Q = \pi[\tfrac{1}{2}D - \delta^*]^2 U_e, \tag{2.1}$$

where D is the exit diameter of the nozzle, U_e is the potential core velocity in the exit plane (found to be uniform except for the boundary layer), δ^* is the displacement thickness associated with the boundary layer at the nozzle exit. The displacement thickness was measured directly, as described in §3. U_e was determined by measuring the pressure drop through the nozzle with a Baratron pressure transducer (Type 370H-10), and using Bernoulli's formula.

A few critical velocity measurements were made using a TSI laser-Doppler velocimeter (LDV) operated in forward-scatter mode; an aerosol of water droplets was used for seeding particle. A hot wire (5 μm diameter, 0.6 mm active length), operated

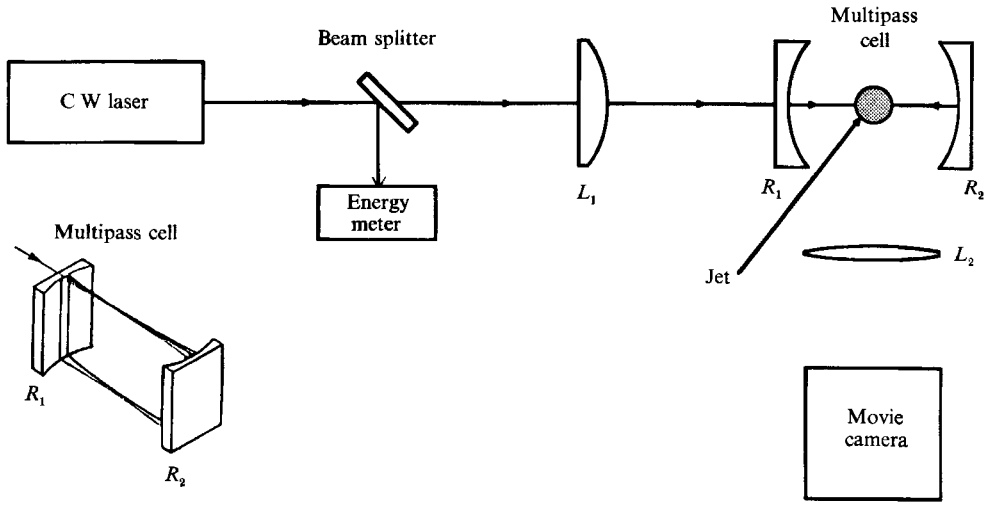

FIGURE 3. Experimental configuration used for obtaining high-speed motion pictures of the aerosol field in a gas jet. Framing speed was 7000 f.p.s. R_1 and R_2 are two concave cylindrical reflectors which create an intense plane of illumination.

on constant temperature mode on the DANTEC 55M01 anemometer, was also used to measure velocity in air jets. In heterogeneous regions, the hot wire cannot, in general, be used for determining the absolute value of the velocity, because the signal E is a function of both velocity $u(t)$ and local helium concentration $c(t)$, i.e. $E = E(u(t), c(t))$. One can always measure the velocity inside the potential core where the fluid is homogeneous, but such probe intrusion can significantly alter the stability characteristics of the oscillating mode (see Sreenivasan *et al.* 1989). Unless otherwise stated, the hot wire was positioned outside the shear layer at $r = \frac{1}{2}D + 5\theta$. It is shown in the Appendix that normalized power spectra obtained at this location are approximately the same as the normalized power spectra of u' obtained inside the potential core, as long as the disturbances are small. Spectral density curves were obtained on a single channel HP Spectrum Analyser (model 3561A). This device displays a discretized spectrum using 400 equal subintervals, or 'lines' to span the desired frequency interval. Several standard spectral windows can be used with the fast Fourier transform (FFT) algorithm. We have always chosen to use a 'flat top' window. A few of the spectral measurements to be reported are concerned with the 'width' of a given peak in the power spectrum. For such measurements, the bandwidth and centre frequency of the spectrum analyser display were adjusted so that the spectral peak spanned a number of lines which was of the order of 10^2. This practice was found to minimize the effects of discretization on this type of measurement.

High-speed motion pictures were made of the jet by illuminating the flow with a narrow sheet of continuous laser light (7 W) in a plane coinciding with the jet axis. Motion pictures were obtained using a Wollensak 'Fastax WF6' 16 mm motion picture camera with 400 ASA movie film. In order to capture several frames within one oscillation cycle, it was necessary to film at high repetition rates, and the film speed ranged up to 7000 s^{-1}. This required intense illumination for adequate quality of the images. The laser sheet was therefore formed using a 'multipass cell' as shown in figure 3. The laser light was reflected back and forth between the two concave cylindrical reflectors creating an intense plane of illumination without ever passing through a

diverging lens. This method is discussed by Long *et al.* (1983). The nozzle fluid was made visible by seeding it with a polydisperse aerosol of water droplets doped with a fluorescent dye (sodium fluorescene). The droplets were generated using a TSI aerosol generator (model 9306). Instantaneous images were obtained using a pulsed Nd:YAG laser. In this case, the laser sheet was formed using a concave cylindrical lens to diverge the beam in the axial plane, and a convex cylindrical lens to converge the beam in the horizontal plane. The laser had a power density of 2×10^7 J s^{-1} per pulse and a pulse duration of about 10 ns. The images were captured on a Photometrics 'IC200' CCD array with a 1300×1035 pixels, and were processed using in-house software (Prasad & Sreenivasan 1990).

3. Governing parameters

Separated free shear flows of heterogeneous composition can potentially depend upon a large number of parameters. However, by limiting the range of flow conditions and by exploiting justifiable approximations, one can construct a set of experiments whose outcome depends upon just a few non-dimensional parameters. We chose at the outset to limit this study to Mach numbers $M = U_e/a_\infty$ less than 0.3; here a_∞ is the sound speed for the ambient air. For most of the experiments, M was substantially smaller. Under these conditions, the Mach number effects are uniformly small. Experiments of Bradshaw (1966) in isothermal air jets suggest the same (see also §5.1); straightforward scaling arguments applied to the full energy equation (Kyle 1991) suggest that this is so also for the variable density case. Thus, the non-dimensional governing equations depend upon the Reynolds number $Re = U_e D/\nu_e$, the Richardson number $Ri = (\rho_e - \rho_\infty) Dg/\rho_\infty U_e^2$, and the Schmidt number $Sc = \nu_\infty/D_{\mathrm{He,air}}$. Here, $D_{\mathrm{He,air}}$ is the diffusivity of helium into air, g is the acceleration due to gravity, and ν_e is the kinematic viscosity of the nozzle fluid, which itself can be calculated using Wilke's (1950) approximation based on the statistical mechanical theory of Chapman–Enskog. In the present experiments, the Richardson number $Ri \leqslant 1.4 \times 10^{-4}$, and so the buoyancy effects are negligible (Kotsovinos 1975). Further, although Schmidt number effects may not be neglected *a priori*, Sc is not an experimental variable in this study because $D_{\mathrm{He,air}}$ is essentially independent of the relative concentrations of helium and air (Geankoplis 1972).

3.1. *Inflow boundary conditions*

The flow everywhere upstream of the nozzle exit is slow and has uniform composition. Reynolds number similarity therefore assures us that the non-dimensional velocity distribution at the nozzle exit is a unique function of the Reynolds number. Figures 4(*a*, *b*) show radial profiles of the streamwise velocity $U(r)/U_e$ obtained in the separated boundary layer for the 13.3 and the 9.3 mm nozzles, respectively, over the Re range covered in the experiments. The profiles are similar and agree closely with the Blasius profile. For all profiles, δ^*/θ was within $\pm 4\%$ of the Blasius value. Here, θ is the momentum thickness defined by

$$\theta = \int_0^{r_{0.1}} (U(r)/U_e)[1 - U(r)/U_e]\,\mathrm{d}r, \tag{3.1}$$

and δ^* is the equivalent plane displacement thickness defined by

$$\delta^* = \int_0^{r_{0.1}} [1 - U(r)/U_e]\,\mathrm{d}r. \tag{3.2}$$

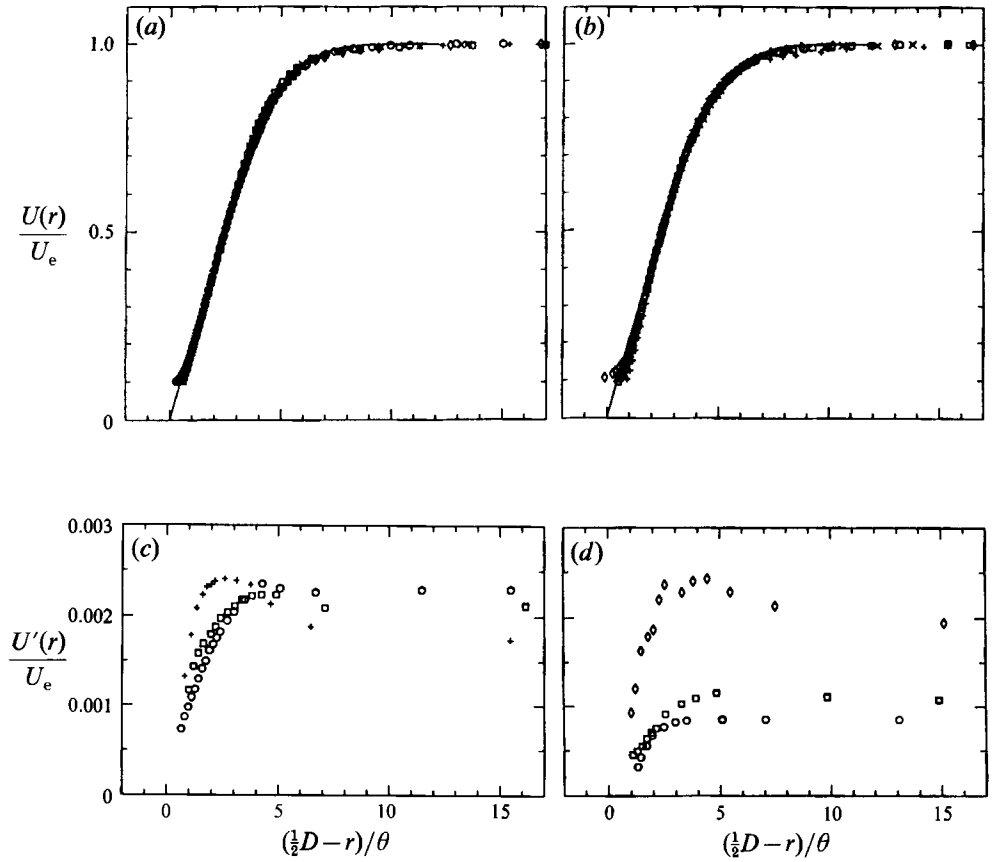

FIGURE 4. Variation of streamwise velocity in the nozzle plane ($x = 0.06$ mm) at various Reynolds numbers: ○, $Re = 16000$; □, $Re = 7000$; ×, $Re = 5000$; *, $Re = 3500$; +, $Re = 2700$; ◇, $Re = 2100$. (*a*) $U(r)/U_e$ for ASME nozzle. $D = 13.3$ mm; (*b*) $U(r)/U_e$ for cubic equation nozzle, $D = 9.3$ mm. (*c*) Fluctuation amplitude u'/U_e for ASME nozzle; $D = 13.3$ mm. (*d*) Fluctuation amplitude u'/U_e for cubic equation nozzle; $D = 9.3$ mm. Measurements are obtained using a standard hot wire in air jets.

The upper limits of integration $r_{0.1}$ signify the location where $U(r)/U_e = 0.1$. The longitudinal velocity fluctuation intensity profiles $u'(r)/U_e$ (figures 4(*c*, *d*)) exhibit peaks at $(\frac{1}{2}D-r)/\theta = 3$, this being typical of jets with initially laminar shear layers (Hussain & Zedan 1978). Centreline values $u'(0)/U_e$ at various speeds U_e were in the range 0.08–0.19% in the 9.3 mm cubic equation nozzle, and 0.17–0.23% for the 13.3 mm ASME nozzle. Both the mean and fluctuating velocity data indicate that the boundary layers separating at the lip of the nozzle are laminar over the *Re* range considered. Because the separated boundary layers are laminar, and their shapes are essentially invariant, the parameter θ fully characterizes the normalized velocity profiles, so that an appropriate non-dimensional ratio is D/θ. Figure 5 shows D/θ values calculated from the above profiles. For all the data presented here, D/θ will be reported – from which the corresponding value of *Re* can be found from figure 5.

The jet is isothermal, as confirmed by direct measurements. The density ratio $S = \rho_e/\rho_\infty$ is therefore just equal to the ratio of the molecular weight of the helium/air mixture to that of air since, for low Mach numbers, the effect of pressure on the density is negligible. With these assumptions, it is easy to show (Kyle 1991) that all other (non-

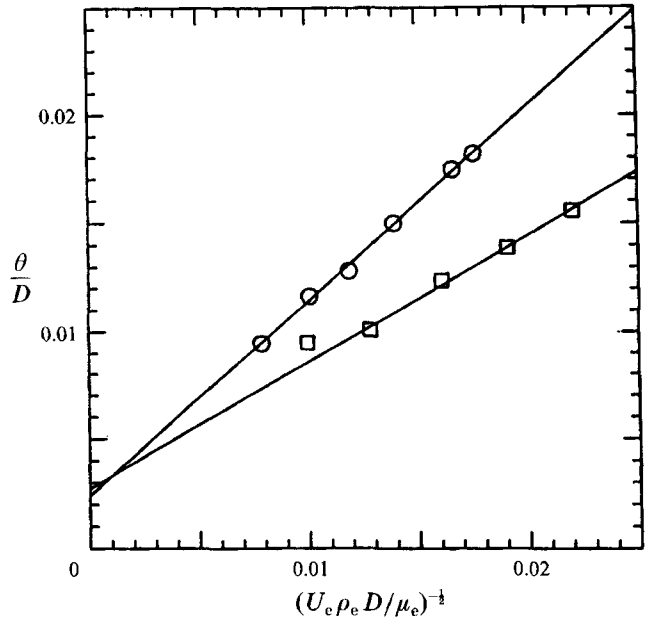

FIGURE 5. Momentum thickness θ/D as a function of the Reynolds number Re: ○, 13.3 mm ASME nozzle; □, 9.3 mm cubic equation nozzle.

dimensionalized) thermophysical properties of the nozzle fluid, such as the kinematic viscosity ratio ν_e/ν_∞ are uniquely specified by S.

3.2. *Overall parameter dependence*

The analysis so far suggests that all non-dimensional characteristics of the flow should depend primarily upon the global parameters D/θ, S and Re. A major goal of this paper is to evaluate the dependence of the oscillating mode of these three global parameters. As we are interested in the growth of small disturbances in the near field, it is also important to take account of the effects of the time-dependent disturbances imposed on the flow. These are due to acoustic noise and to vortical disturbances originating upstream of the nozzle. Such background disturbances may, under certain circumstances, strongly affect the flow, though they may be weak (Cohen & Wygnanski 1987; §5 of present paper).

Finally, it is of interest to note that in the limit $Re \to \infty$ and $M \to 0$, the system of equations and boundary conditions governing the heterogeneous, isothermal flow is analogous to those governing the heated air jet (Brown & Roshko 1974; Kyle 1991). Whenever possible we shall compare our measurements with results obtained by Monkewitz *et al.* (1989, 1990) and Raghu & Monkewitz (1991) in heated air-jet experiments for similar values of D/θ and S.

4. Evolution of highly organized structures in the near field

Before proceeding further, it is helpful to have an overall kinematical description of the transition from organized to disorganized states in variable-density jets. At the instant shown in figure 2(*a*), an axisymmetric wave appears close to the nozzle and is followed by two vortex rings in the streamwise direction; beyond this, the nozzle fluid necks down and finally 'pinches off', leading to a disorderly structure downstream. A

D/θ	92	69	69	**69**	60	60	**60**	50	**50**
S	1.0	0.66	0.48	**0.29**	1.0	0.58	**0.48**	0.48	**0.29**
λ/θ	38	37	35	**44**	36	31	**38**	37	**39**
L/θ	125	120	85	**67**	132	146	**75**	110	**47**

TABLE 1. λ/θ and L/θ as measured directly from the films: $D = 13.3$ mm. Values represent an average of 100 successive eddies. Jets dominated by the oscillating mode are indicated in bold print.

region of fluid having a relatively low concentration of nozzle gas surrounds the disorderly structure and extends beyond the range of the image. In order to study the history and interaction of these structural elements, high-speed motion pictures have been made of the transition region of the jet issuing from the 13.3 mm nozzle for nine different combinations of the governing parameter S, D/θ and Re. The density ratios range from unity (air into air) down to $S = 0.14$ (pure helium into air) while D/θ lies roughly between 50 and 91 (see table 1). LDV measurements are correlated with the films for the same flow conditions. The results of this effort are summarized below.

4.1. *General observations*

In certain visual respects, the evolution of large-amplitude structures was found to be similar for all nine flow conditions considered. Instability waves which form in the initially laminar shear layer are always axisymmetric; between 1 and 2.5 diameters downstream of the nozzle, these waves fold or 'break' and quickly roll up to form a train of vortex rings, the centres of which continually move downstream. These are the vortex ring structures seen in figure 2(*a*). When the oscillating mode is present, each vortex ring is involved in exactly one pairing inside the viewing region ($0 \leqslant x/D \leqslant 4.75$), whereas in jets not supporting the oscillating mode, the interaction is less repeatable and a vortex ring occasionally passes from view without coalescence.

The pairing process itself can be seen in the sequence of ten successive movie frames of figure 6. These frames advance from left to right, with the left-most frame in the bottom row immediately following the last frame in the top row. By comparing frames 1 and 6, 2 and 7, and so forth, it is seen that the overall structure in the transition region repeats itself to a remarkable degree; even the fine structure downstream of the potential core termination repeats for many cycles. It is evident that the processes involved in the growth, interaction and breakdown of vortices all evolve temporally in a periodic fashion.

While these pictures are quite instructive, they do not tell the whole story: flow visualization experiments in constant density jets also show some repeatability of structure interactions at low Reynolds numbers below about 10^4 (Becker & Massaro 1968; Browand & Laufer 1975; Davies & Baxter 1977). However, for nozzle Reynolds numbers of the order 10^5 and above, there is much less repeatability in constant-density jets; further, the initial instability of the laminar shear layer could be both axisymmetric and helical (Browand & Laufer 1975; Drubka & Nagib 1981) – quite unlike the situation here.

The differences between the two classes of jets are quantified in the remaining subsections.

4.2. *The disturbance wavelength and wave-breaking length*

Two lengthscales which characterize the disturbances in a shear layer are: (i) the wave-breaking length, L, and (ii) the disturbance wavelength, λ. These are defined in figure 7. Their values, as deduced from the high-speed motion pictures, are summarized in

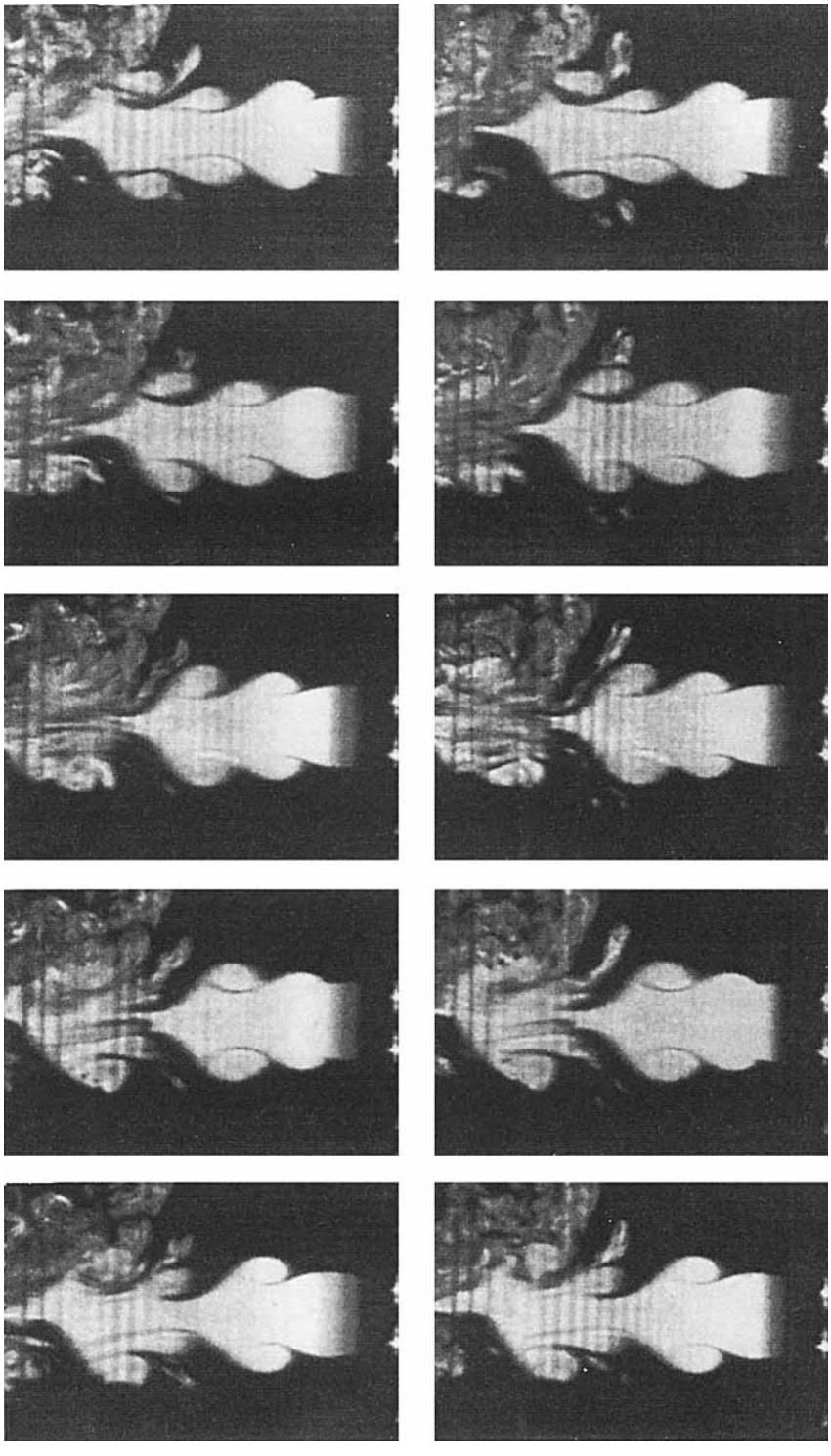

FIGURE 6. Successive movie frames showing the aerosol distribution in an axial plane of a seeded flow. $S = 0.29$; $D/\theta = 50$; $Re = 3025$; $D = 13.3$ mm. The sequence proceeds from left to right and from top to bottom. Framing rate $= \frac{5}{2} f_0$. The horizontal bands in the photographs are artifacts of using the multipass cell (see figure 3).

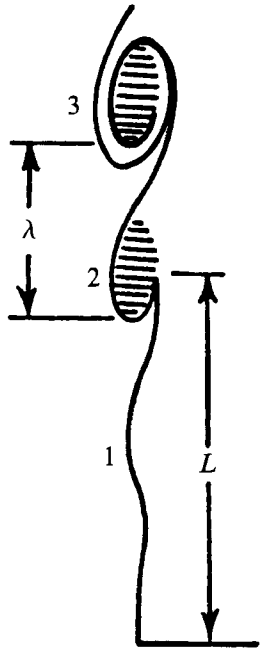

FIGURE 7. Typical pattern of disturbance evolution (after Becker & Massaro 1968).

table 1, where the data have been non-dimensionalized using θ. Each entry represents the average data on 100 successive vortices.

For flows which do not support the oscillating mode, λ/θ values shown in table 1 vary about a mean of 35.7 with a standard deviation of about 2.3. This variation appears random, hence λ/θ appears to be essentially independent of D/θ and S in the ranges considered. We note that the inviscid linear theory of Michalke (1971) indicates that, at $D/\theta \approx 69$, the most spatially amplified mode for $S = 1.0$ has a wavelength $\lambda/\theta \approx 33$. Furthermore, the analysis indicates that λ/θ is only weakly dependent upon D/θ and S; for example the most spatially amplified mode at $D/\theta \approx 69$ for $S = 0.50$ has wavelength $\lambda/\theta \approx 34$. These theoretical results are in good quantitative agreement with the data shown in table 1 for jets which do not sustain the oscillating mode.

For flows which do support the oscillating mode, λ/θ differs significantly from the values just discussed. At $D/\theta = 69$, S is reduced from 0.48 to 0.29, which encompasses the boundary for the onset of the oscillating mode, and λ/θ increases from 35 to 44. This suggests that the characteristics of the oscillating mode differ from other shear-layer modes. Measurements of the passage frequency presented in § 5 will show that this is indeed the case.

The L/θ values presented in table 1 show a marked distinction between the range of wave-breaking lengths in flows which sustain the oscillating mode and those which do not. For $D/\theta = 50$ and 60, reductions in S also correspond with reductions in L/θ (by 57% and 48%, respectively). The implication is that the instability waves break much closer to the nozzle in the presence of the oscillating mode. Physical intuition suggests that the wave-breaking length depends upon both the streamwise amplification rate of the instability waves as well as their 'initial' intensity. In § 5 it will be shown that the intensity of the oscillating mode is indeed closely associated with its large initial value.

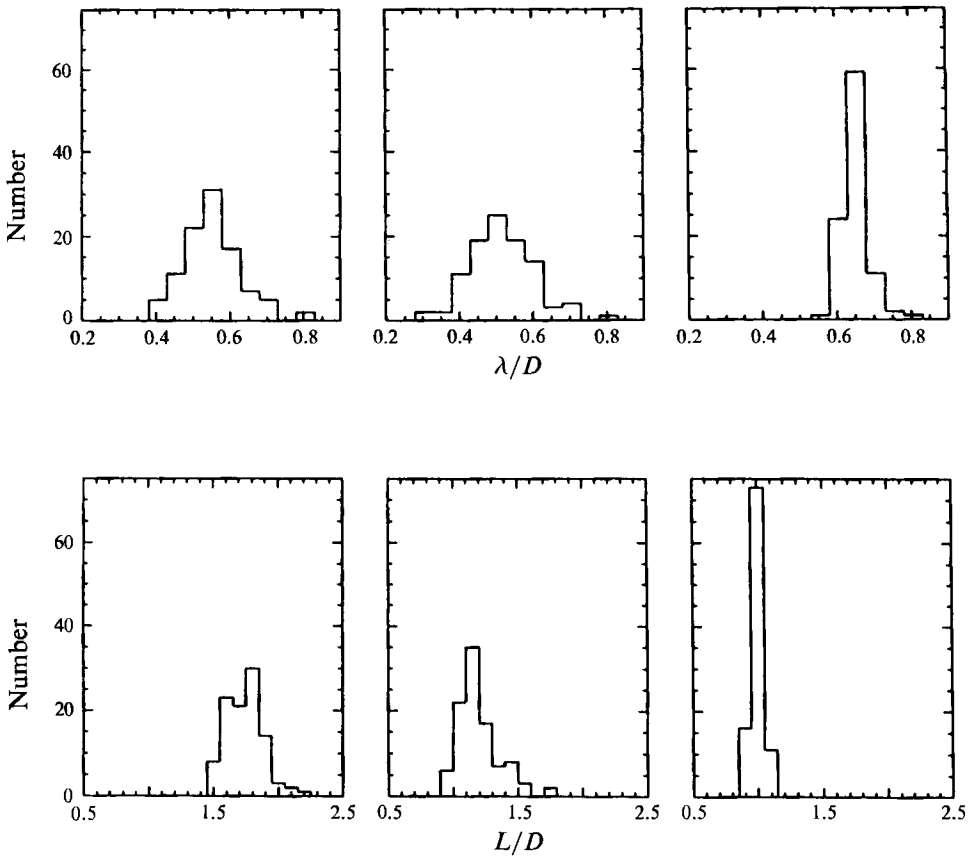

FIGURE 8. Histograms of wavelength λ/D and wave-breaking length L/D for various S: $D/\theta = 69$; $Re = 5500$; $D = 13.3$ mm; sample size = 100. From top left to bottom right: $S = 0.66$, $\sigma = 0.08$ (σ here is the standard deviation for the histogram); $S = 0.48$, $\sigma = 0.09$; $S = 0.29$, $\sigma = 0.04$; $S = 0.66$, $\sigma = 0.14$; $S = 0.48$, $\sigma = 0.16$; $S = 0.29$, $\sigma = 0.05$.

4.3. *Orderliness in kinematics*

Figure 8 shows histograms of λ/D and L/D for three different values of S, for $D/\theta \approx 69$. The standard deviation, σ, characterizing the uncertainty in the measurement of any single passing structure was estimated to be $\pm\frac{1}{20}D$. It is seen that σ for the wavelength data is roughly twice for $S = 0.66$ and 0.48 than that for $S = 0.29$. Recall from table 1 that at $D/\theta \approx 69$, the oscillating mode dominates the transition region for $S = 0.29$, and is absent at $S = 0.66$ and 0.48. The standard deviation for the wave-breaking length is roughly three times larger for $S = 0.66$ and 0.48 than that for $S = 0.29$. These results indicate that, for flows dominated by the oscillating mode, unusual regularity exists in the wavelength and in the location where the wave-braking process begins.

In figure 9, the locations of twelve successive eddies are followed from frame to frame for $S = 0.66$ and $S = 0.29$, with $D/\theta \approx 69$. The trajectory of each individual eddy is plotted from the wave-breaking point to the point where coalescence begins (see figure 6). Once individual vortices begin to wrap around their neighbours, their location can no longer be tracked. Focusing first on $S = 0.66$, it is seen from the first point of each trajectory that wave breaking occurs randomly in time (location along the abscissa) as well as in space (location along the ordinate). This result is expected

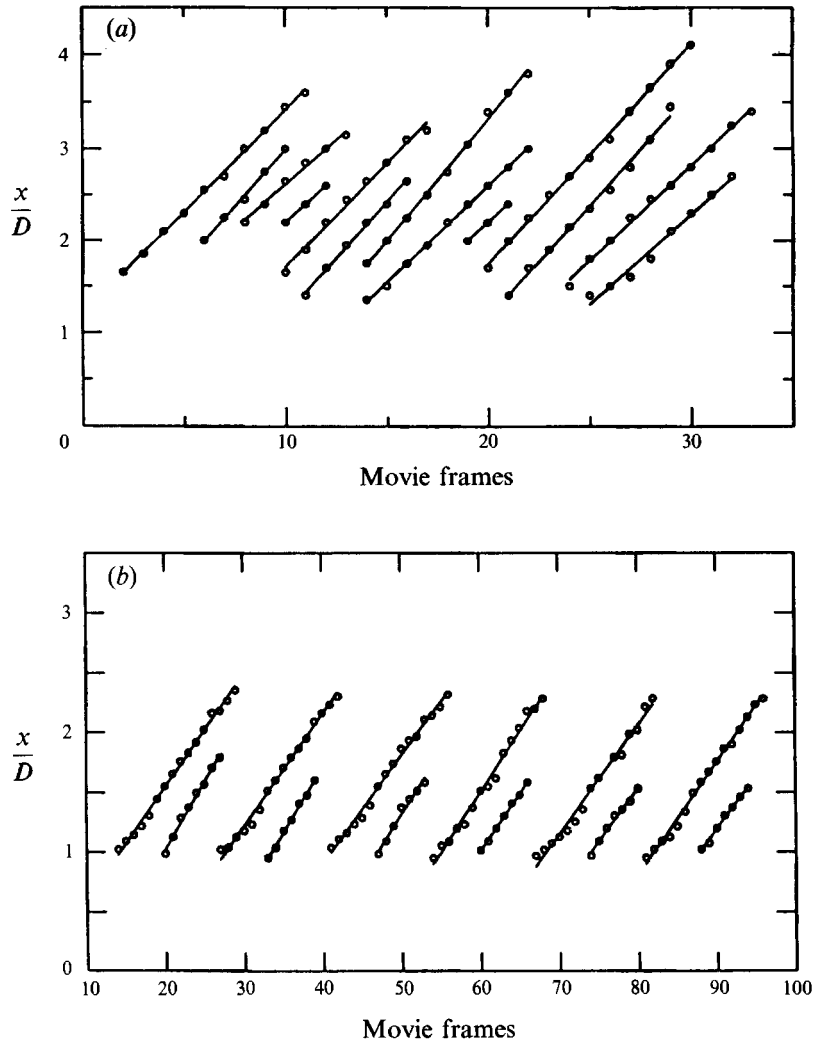

FIGURE 9. Eddy trajectories: $D/\theta = 69$; $Re = 5500$; $D = 13.3$ mm. Each trajectory begins where the wave 'breaks' and ends at the start of the coalescence process. Straight lines are least-squares fits. (*a*) $S = 0.66$. (*b*) $S = 0.29$.

from the histogram of L shown in figure 8 for the same conditions. From the final point of each trajectory it is seen that the coalescence process also exhibits significant random variation. For $S = 0.29$, however, both the roll-up and the coalescence are quite regular (see also figure 8). Such regularity is exhibited in all of the jets which support the oscillating mode. From the combined facts that pairing induces complete pinching off of potential core fluid, and that this process occurs with extreme regularity, one might expect that an axial profile of the time-averaged nozzle fluid concentration should exhibit a very sharp drop in the region where this process occurs. This is in fact the case (see also Chriss 1968; Tombach 1969).

Notice that the framing rate in the films was adjusted to be such that the duration for ten frames coincided with the subharmonic. This orderliness seen in figure 6 shows that the entire flow field approximately repeats itself after every subharmonic period.

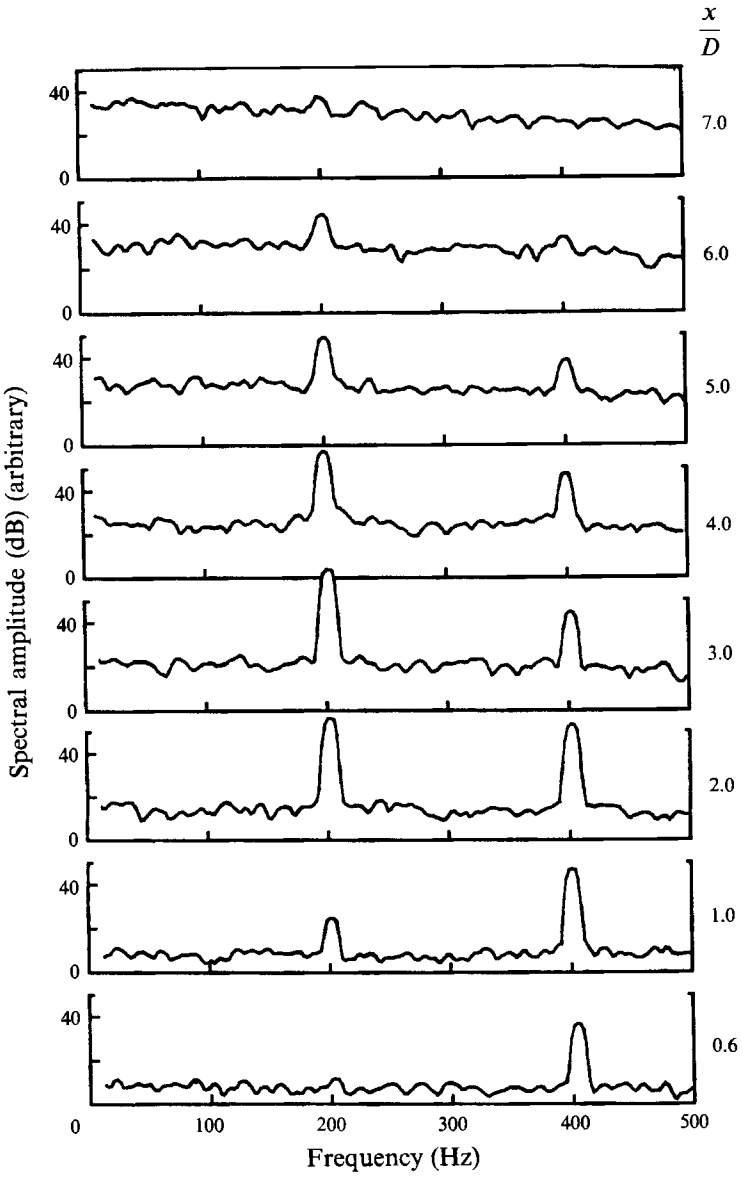

FIGURE 10. Power spectra of u' at various axial locations: $S = 0.29$; $D/\theta = 50$; $Re = 3025$; $D = 13.3$ mm. The corresponding x/D are marked on the curves. Spectra are calculated from time traces obtained using LDV.

4.4. *Centreline velocity*

The longitudinal component of velocity has been measured at various streamwise locations along the centreline using the LDV set-up mentioned in §2. Possible effects of seeding on the flow were investigated by monitoring the change in the frequency of the oscillating mode. The frequency as measured by a hot wire outside the shear layer never differed from the seeded case by more than 2%. A data rate of 10000 s^{-1} allowed us to construct a reasonable time trace, from which the spectra shown in figure 10 were calculated for $S = 0.29$ and $D/\theta = 50$. In figure 11, the spectral intensities of the

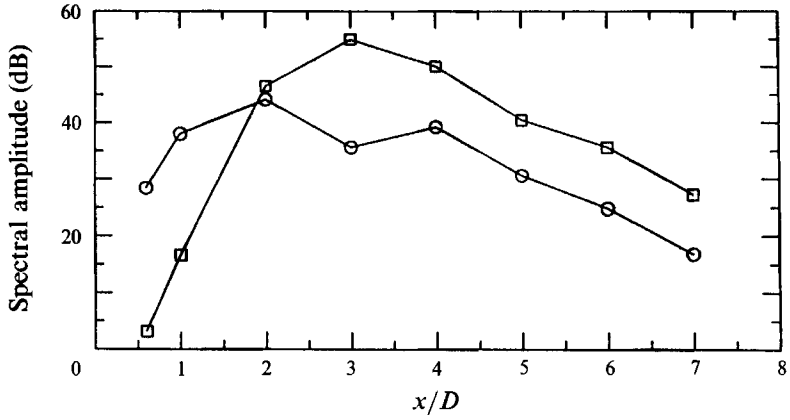

FIGURE 11. Spectral amplitudes for the fundamental and the subharmonic seen in figure 10: ○, fundamental; □, subharmonic.

primary and subharmonic modes are shown explicitly as functions of x/D. Notice that the ordinate in figure 10 is compressed and the abscissa is expanded (say, relative to figure 1) so that the spikiness of the spectral peaks is not apparent at a cursory glance.

It is useful to correlate the spectral intensities in figures 10 and 11 with the motion of the flow structures. At $x/D = 0.6$, the power spectrum exhibits a single peak. The frequency of this mode corresponds with the average local passage frequency of the initial axisymmetric wave. This is the fundamental mode, which continues to grow in intensity along the centreline even as the waves seen in the films break and roll up. The subharmonic appears in the spectra at around $x/D = 1$, and attains its maximum intensity along the centreline at $x/D = 3$. It is seen in the films that this maximum occurs at a location where fluid along the centreline is rapidly accelerated during the pinching off process, which, of course, occurs once every subharmonic period. Beyond $x/D = 3$ all discrete modes in figures 10 and 11 continually decay in the streamwise direction until, at $x/D = 7$, the subharmonic is barely discernable above the background. Correspondingly, the remnant of the pairing process appears in the film to become more diffuse as it travels downstream of $x/D = 3$.

Figure 12 shows the centreline profiles of the root-mean-square (r.m.s.) velocity u'/U_e and the mean velocity U/U_e for $S = 1.0$ and 0.29, and for $D/\theta \approx 50$. For reference, note that these are the same conditions as for figures 6, 10 and 11. The centreline turbulence intensity for $S = 0.29$ attains much larger amplitude compared with the air jet ($S = 1$). To our knowledge, such large intensities of the order 0.3 do not occur in an unforced constant-density jet. The peak u'/U_e value occurs at $x/D = 3.0$, which also corresponds with the peak in the subharmonic mode (figure 11). Thus, the abnormally large velocity fluctuation found in this jet is primarily associated with the vortex pairing process. U/U_e is seen to fall off rapidly starting from a diameter or so from the nozzle. On the other hand, we have already mentioned in §4.3 that the density of the gas along the centreline is approximately uniform until the pinching-off starts at about $x/D = 2.5$. In the region $1.0 \leqslant x/D \leqslant 2.5$ slow, dense ambient air is being engulfed by the roll-up process, but this mixing does not penetrate to the centreline. The attenuation of U/U_e therefore implies the existence of an adverse streamwise pressure gradient.

In summary, the breakdown of the highly organized motion near the nozzle occurs in a qualitatively similar manner in all jets with $50 \leqslant D/\theta \leqslant 100$ and $0.6 \leqslant S \leqslant 0.14$, and is characterized by the growth of axisymmetric instability waves in the initially

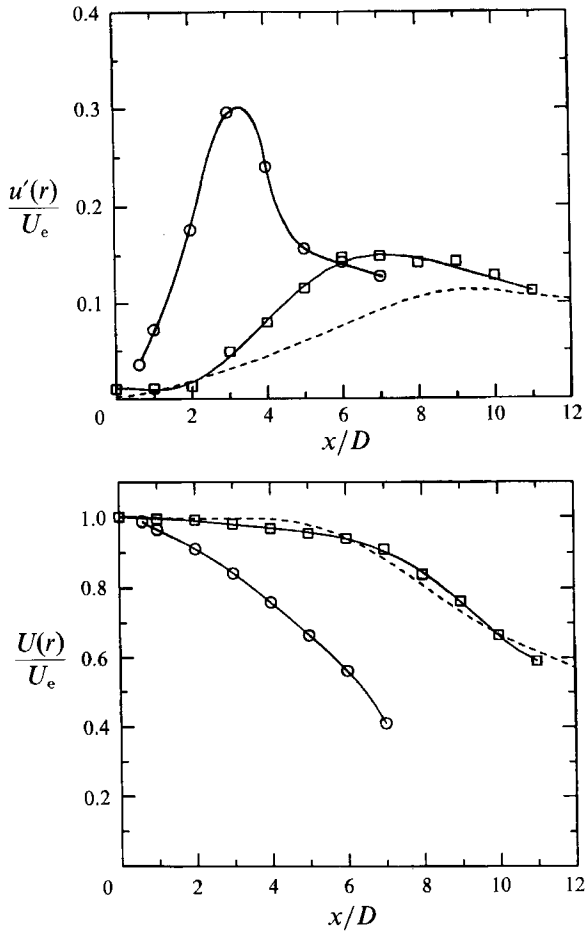

FIGURE 12. Streamwise component of the root-mean-square and the mean velocity as a function of x/D: ○, $S = 0.29$; □, $S = 1.0$; $D/\theta = 50$; $Re = 3025$; $D = 13.3$ mm. ——, Corrsin & Uberoi (1949).

laminar shear layer; they pair and pinch off the potential core. The unique features of the oscillating mode are the following: (i) their wavelengths are not well predicted by linear stability theory (§4.2); (ii) waves break very close to the nozzle (§4.2); (iii) at each point in the near field, the flow is highly organized around the subharmonic period (§4.3); and (iv) fluctuations are intense and interact strongly with the mean flow field (§4.4).

5. The dynamical aspects of the near field

In this section, properties of the oscillating mode are studied at short downstream distances $x/\theta \leqslant 75$. We make use of power spectral density curves obtained from a hot wire located outside the shear layer, where these curves are representative of the power spectrum for the streamwise velocity inside the shear layer (see Appendix). These near-field measurements will be used in §§5.1, 5.2 and 5.3 for the purpose of studying the evolution of the oscillating mode with respect to the global parameters Re, D/θ and S. When cast in dimensionless form, this behaviour may be meaningfully compared with the theory of absolute instability.

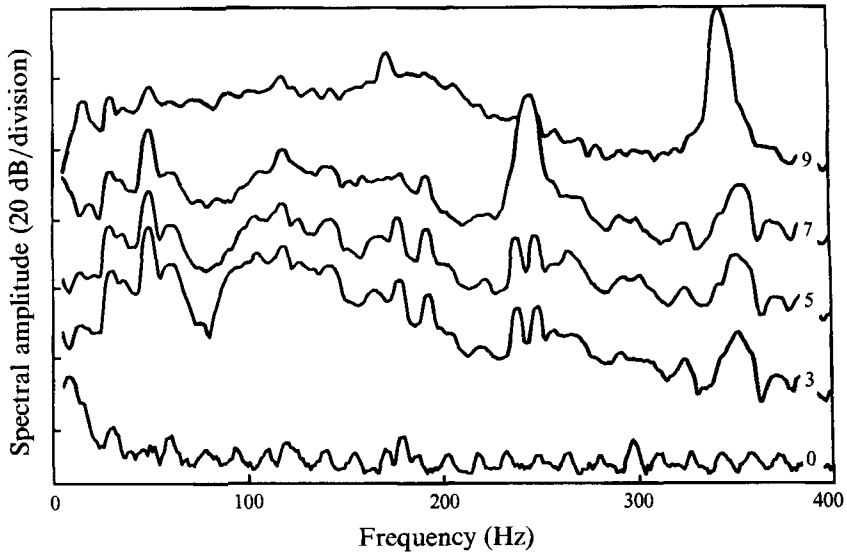

FIGURE 13. Power spectra of u' at various jet velocities U_e: $S = 0.29$; $x/D = 0.10$. Spectra are labelled with U_e in ms^{-1}. The arbitrary reference for the dB scale varies from curve to curve.

5.1. *Modal variations with S fixed*

We emphasize that in quantitative studies reported in this paper, one parameter at a time was varied keeping others fixed. The first section is meant to illustrate the qualitative changes which occur in the power spectrum by steadily varying the jet velocity while holding the nozzle gas density constant.

Figure 13 depicts these qualitative changes for $S = 0.29$ as the exit velocity is varied from 3.0 to 9.0 m/s. Note that the spectral distributions corresponding to 3.0 and 5.0 m/s are similar in that their peaks occur at identical frequencies. This frequency invariance was also exhibited in power spectra of u' obtained by Cohen & Wygnanski (1987) inside the shear layer at $x/D \approx 0$ for air jets. They suggested that the (relatively weak) spectral peaks could be attributed to the acoustic resonance properties of the upstream plenum chamber, which are of course dependent only upon the cavity geometry and the sound speed (see also Crow & Champagne 1971). The same conclusion had been reached by Hussain & Ramjee (1976) when they found that neither the shape of the nozzle contour nor variations in D/θ had any effect on the frequency of several spectral spikes both upstream and downstream of the nozzle contraction. These observations imply that the distribution of spectral peaks obtained in the near field of heterogeneous jets – with uniform gas composition upstream of the nozzle – should likewise be independent of the jet velocity, as indeed evidenced in figure 13. We also note that the frequency of fluctuations that are excited by the ubiquitous ambient acoustic signals will be independent of the velocity and density.

When U_e is increased from 5.0 to 7.0 m/s, however, a distinct spectral peak emerges above the background spectral distribution of u'. This is the oscillating mode which, near to its onset, does not appear to influence the intensity of modes at neighbouring frequencies. Such interaction does appear only when the oscillating mode has grown more intense (as in the uppermost spectrum in figure 13 corresponding to $U_e =$ 9.0 m/s). As suggested by figure 13, we have consistently found that the spectral intensity of the oscillating mode increases rapidly and continuously with U_e near its onset, when measured at any fixed location (see also Monkewitz *et al.* 1990). The

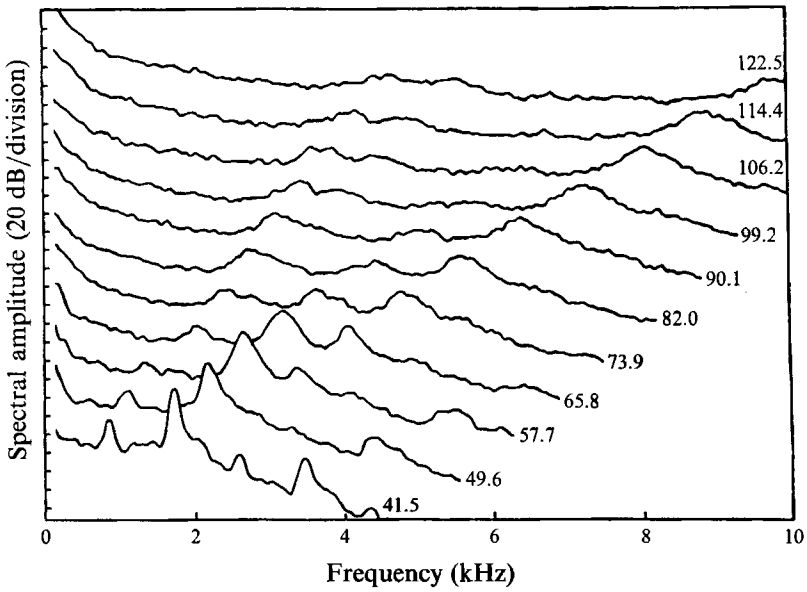

FIGURE 14. Power spectra of streamwise velocity fluctuations u' within the shear layer: $S = 0.14$; $x/D = 0.10$. Spectra are labelled with U_e in ms^{-1}. The arbitrary reference for the dB scale varies from curve to curve.

frequency of the oscillating mode increases monotonically with U_e. Note that because the oscillating mode alone is velocity dependent very near the nozzle, it can be readily distinguished from the background disturbance peaks near to its onset.

Figure 14 shows qualitative changes that occur in the spectral distribution of shear layer disturbances as the velocity is increased above values for which the oscillating mode has already achieved a relatively large intensity. In the spectrum corresponding to $U_e = 41.5$ m/s (at the bottom of figure 14), the tallest peak at $f = 1733$ Hz is the fundamental of the oscillating mode. Its subharmonic and several higher harmonics are also evident. Between $U_e = 49.6$ m/s and 65.8 m/s (second and fourth spectra from the bottom) the velocity evolves from a stable periodic state to one dominated by disturbances with relatively broadband spectral content. Note that although the pure periodicity is lost, these relatively broadband disturbances are still to be regarded as the oscillating mode, simply because the frequency and intensity change smoothly with U_e. This transition has been discussed by Kyle & Sreenivasan (1988, 1989) and Monkewitz *et al.* (1990). In this same velocity range, the subharmonic of the oscillating mode diminishes in intensity at this streamwise location and finally vanishes. As the velocity increases above 65.8 m/s (fourth spectrum from the bottom), the oscillating mode diminishes in amplitude and finally disappears.

At about 57.7 m/s (third spectrum from the bottom) two other broadband modes emerge with frequencies which differ by approximately a factor of two. Their frequencies are apparently not related to that of the oscillating mode. As the velocity increases above 57.7 m/s, these modes intensify. It may be thought that compressibility affects the disappearance of the oscillating mode or the emergence of these other broadband modes, since $M^2 = 0.126$ for the uppermost spectral density. However, this is almost certainly not so because they occur at $M^2 = O(10^{-2})$ for $S = 0.29$ and $M^2 = O(10^{-3})$ for $S = 0.48$ (see §5.2). The possibility of Mach-number dependence will therefore not be further mentioned.

Our measurements were made over a six-year period using several settling chamber configurations, four nozzles with differing contraction contours and relate to the following parameter ranges: $0.14 \leqslant S \leqslant 1.0$; $40 \leqslant D/\theta \leqslant 125$; $800 \leqslant Re \leqslant 15000$. On the basis of data obtained from films (§4), centreline LDV measurements (§4) and near field hot-wire measurements described in this section so far, we conclude that the only modes that are sustained in our facility, which are unique to helium/air jets, are: (i) the oscillating mode, along with its subharmonic and higher harmonics, and (ii) the broadband modes evidenced in figure 14 at higher values of D/θ and Re.

Monkewitz *et al.* (1990) have reported that the heated air jet will support two distinct oscillatory instabilities having unrelated frequencies, which they call 'Mode I' and 'Mode II'. The bulk of their observations pertain to 'Mode II'. We note that kinematic features of their 'Mode II' are similar to those of the oscillating mode. In spite of the existing uncertainty about the parameters governing these instabilities, there appears to be good agreement between the S range for 'Mode II' ($S \leqslant 0.62$) and for the oscillating mode ($S \leqslant 0.61$), as well as between the $St_D = fD/U_e$ values for the two modes (≈ 0.45). The oscillating mode, like 'Mode II', was determined by experiment to be axisymmetric. From these comparisons, and others to be developed further in §§5.2, 5.3, it is reasonable to suppose that 'Mode II' supported in heated jets and the oscillating mode in He/air jets are essentially the same.

Little is known about the physical nature of these broadband modes; for example, we have not determined their azimuthal dependence. It is not known whether they occur in heated air jets, because Monkewitz *et al.* did not examine U_e beyond where 'Mode II' (the oscillating mode) began to broaden, whereas it is precisely at these U_e values that the broadband modes first appear in He/air jets (figure 14). As to the possible correspondence of these modes with 'Mode I' of Monkewitz *et al.*, it should be noted that 'Mode I' is very 'spiky' whereas the broadband modes, by definition, are not. Furthermore, at any given S, 'Mode I' occurred in the facility of Monkewitz *et al.* at only the small U_e values (small D/θ and Re), whereas the broadband modes were observed in our facility only at high speeds (large D/θ and Re). We tentatively conclude that the 'Mode I' instability does not occur in helium/air jets.

5.2. *D/θ dependence of the frequency of the oscillating mode*

The principle of dynamic similarity assures us that when fluctuation frequencies are expressed in non-dimensional form, their values must depend only upon D/θ, Re and upon background disturbances, if S is fixed. For the case of fixed nozzle gas composition these parameters cannot be varied separately using a single nozzle. In order to examine whether the Strouhal number $St_D = fD/U_e$ is a function of either D/θ or Re alone, data obtained in both the ASME nozzle and in the cubic equation nozzle are plotted together in figure 15. It is assumed that difference in the exterior geometry of the nozzle lips are not significant enough to affect the results. St_D values for the two jets are quite disparate when plotted as a function of Re (figure 15*a*), where they match well when plotted as a function of D/θ (figure 15*b*). Re values in each jet differ by approximately a factor of 2.3 at each D/θ over the range of interest; the maximum initial shear-layer disturbance levels (u'/U_e) for fixed D/θ values differ in the two nozzles by a factor of about 2.2. It follows that, to within experimental error, non-dimensional frequencies for the oscillating mode – as well as for other modes sustained at large D/θ – are dependent upon D/θ alone over the parameter range of interest, and that the Reynolds number is felt only indirectly through its influence on D/θ. Subbarao (1987) studied an oscillating mode in buoyant helium jets ($0.08 \leqslant Ri \leqslant 0.79$) having fully-developed parabolic velocity profiles at the nozzle exit ($D/\theta = 15$), and found that

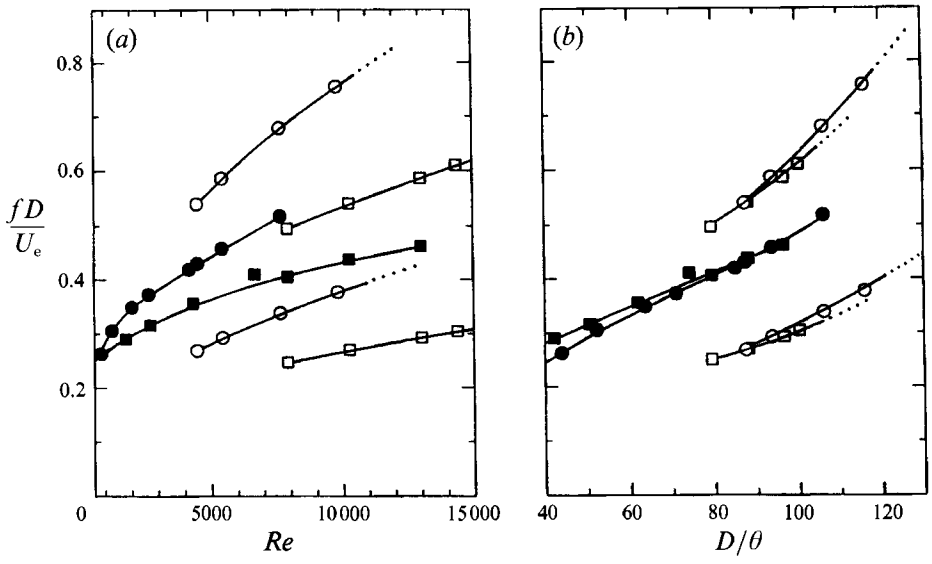

FIGURE 15. Non-dimensional frequency fD/U_e plotted separately as a function of D/θ and as a function of Re: ○, $D = 9.3$ mm; □, $D = 13.3$ mm. $S = 0.14$; $x/D = 0.10$. Solid symbols represent the oscillating mode; open symbols represent the other broadband modes prevalent in the near-field measurements (see figure 14).

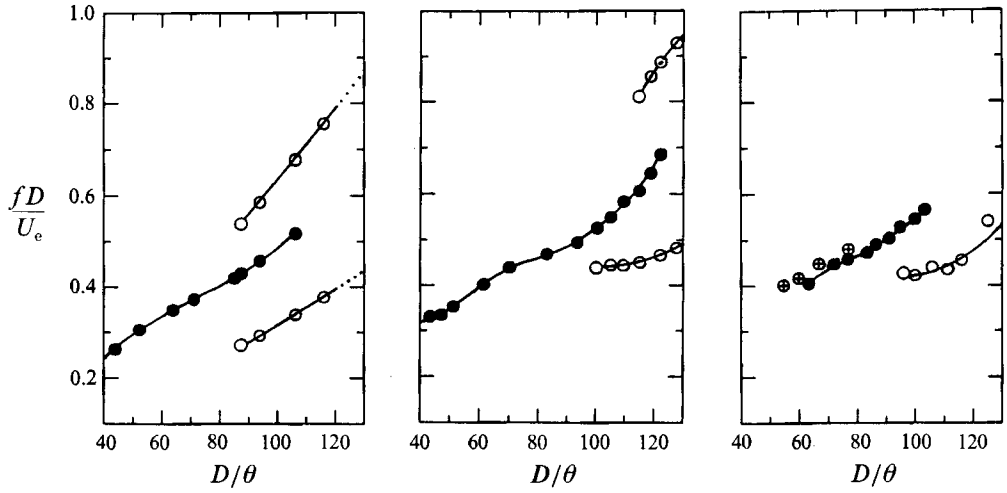

FIGURE 16. Non-dimensional frequency fD/U_e as a function of D/θ for various values of S: $x/D = 0.10$; from left to right $S = 0.14$, 0.29 and 0.48 respectively. ●, oscillating mode from present experiments; ○, additional prominent disturbance modes in present facility; ⊕, oscillating mode (Mode II) in the heated air jet (Monkewitz *et al.* 1990).

St_D was independent of Re ($1500 \leqslant Re \leqslant 12500$). However, it is unclear how relevant his results are to the current ones, as the parameter ranges for the two studies are different.

In figure 16, the non-dimensional fluctuation frequencies shown in figure 15 for $S = 0.14$ are replotted along with similar data obtained for $S = 0.29$ and $S = 0.48$. It is seen that as S changes, the functional relation between the near-field stability characteristics and D/θ also changes. The lower onset value of D/θ for the oscillating mode is about 40 for $S = 0.29$ and about 60 for $S = 0.48$, whereas for $S = 0.14$ it

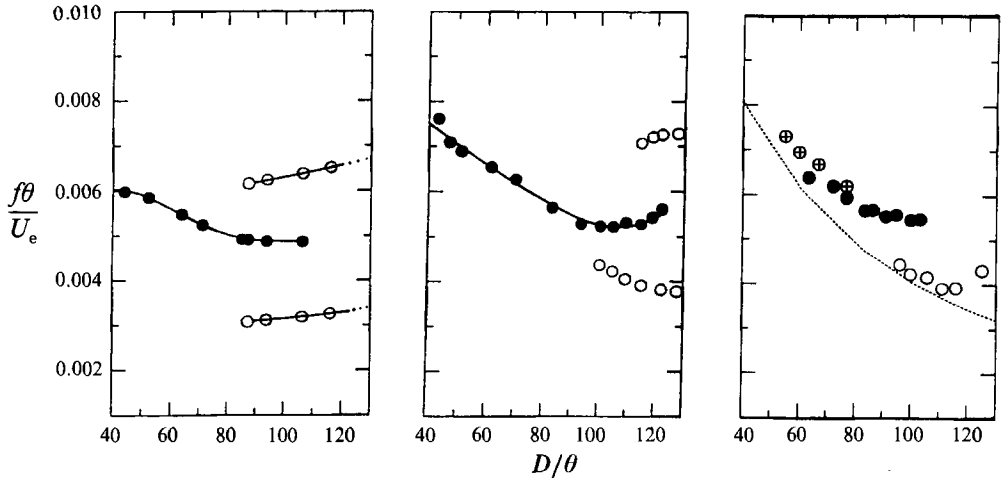

FIGURE 17. Non-dimensional frequency $f\theta/U_e$ as a function of D/θ: $x/D = 0.10$; ●, oscillating mode from present experiments; from left to right $S = 0.14$, 0.29 and 0.48 respectively. ○, additional prominent modes in present facility; ⊕, oscillating mode in the heated air jet (Monkewitz *et al.* 1990); – – – –, theory (Monkewitz & Sohn 1988).

extends below 40, and could not be ascertained. A qualitative feature common to all three density ratios is that the oscillating mode vanishes when D/θ becomes large enough. At least one of these new modes always persists beyond the D/θ bounds for this study. Experimental data obtained by Monkewitz *et al.* (1990) in a heated air jet with $S = 0.47$ are plotted along with helium/air jet data for $S = 0.48$. D/θ ratios were calculated assuming the vorticity thickness $\delta_\omega = 5\theta$ for the initial velocity profile in the heated air jet of Monkewitz *et al.* (1990). It is seen that the comparison is very good indeed, even though at each D/θ, Re differs by roughly a factor of 2 and the two flows are not strictly analogous. This confirms the correspondence between 'Mode II' in heated jets and the oscillating mode in helium/air jets.

The broadband modes that appear when D/θ reaches large values – one or two, depending on the density ratio – do not correspond to 'Mode I' of heated air jets in terms of the frequency range ($0.25 \leqslant St_D \leqslant 0.3$) as well as density ratio ($0.55 \leqslant S \leqslant 0.69$).

The frequency data shown in figure 16 have been non-dimensionalized using the momentum thickness as the lengthscale, and the resulting $St_\theta = f\theta/U_e$ values are plotted in figure 17. It is clear that f scales neither on D nor on θ within the D/θ range covered. In order to find out whether f scales 'more closely' on θ or D, we have evaluated $\Delta(St_D)/(St_D)_{max}$ for each of the curves in figure 16, where $\Delta(St_D)$ is the range in any one curve and $(St_D)_{max}$ is the maximum value in the same curve, and compared these ratios with $\Delta(St_\theta)/(St_\theta)_{max}$ calculated from figure 17. At each S, the ratio for St_θ is approximately half as large as for St_D. Further, much of the variation in St_D occurs for D/θ values above 80 (figure 16), whereas St_θ variations are small in this region (figure 17). This suggests that as the shear-layer thickness becomes small relative to the diameter, the shear-layer thickness tends to play a more dominant role in establishing the frequency of the oscillating mode. The relative invariance of St_θ was not observed in our previous study (Kyle & Sreenivasan 1989) because of the limited D/θ range considered.

Another important feature emerges from figure 17. The frequency of the stationary mode, $\omega_r(k^*(0))$, as calculated by Monkewitz & Sohn (1988), is compared with the

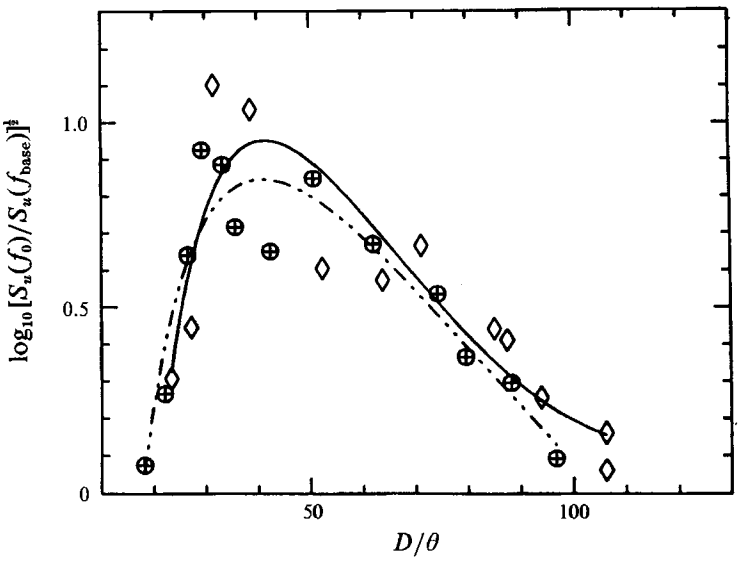

FIGURE 18. Near-field base-to-peak intensity as a function of D/θ: —— ◇, $D = 13.3$ mm; – – – – ⊕, $D = 9.3$ mm. $S = 0.14$; $x/D = 0.10$. Corresponding Reynolds numbers are shown in figure 15. (See text for definitions.)

experimental data for $S = 0.48$. The correspondence seems reasonably good for smaller D/θ, but degrades as D/θ is increased. The Strouhal number of the broadband modes also agrees with the theory for a range of D/θ. The spatial theory predicts that the most unstable mode for $S = 0.5$ should have $0.0125 \leqslant St_\theta \leqslant 0.013$ for this range of D/θ (Michalke 1984), which is clearly a poor prediction.

5.3. *The intensity of the oscillating mode*

We turn our attention to the intensity of the oscillating mode. Specifically, we are interested in choosing a non-dimensional measure of intensity which will reflect the transition that the oscillating mode undergoes from a pure periodic disturbance to one with a relatively broadband spectral content (see figure 14). One possible measure is the ratio of the maximum intensity on the spectral peak, located at f_0, so the intensity at the base of the peak. The 'base' is arbitrarily chosen to be wherever the width of the spectral peak, measured in Hertz, is equal to $\frac{1}{10}f_0$. Thus, letting $S_u(f)$ denote the power spectral density of u' at frequency f, we define the base-to-peak intensity as $[S_u(f_0)/S_u(f_{\text{base}})]^{\frac{1}{2}}$. This measure of base-to-peak intensity is generally greatest whenever velocity fluctuations associated with the oscillating mode are simultaneously intense relative to background disturbance, and distributed over a spectral bandwidth smaller than $\frac{1}{10}f_0$.

In figure 18, the near-field base-to-peak intensities for jets issuing from each of the nozzles are plotted as functions of D/θ for $S = 0.14$. The curves correspond to fourth-order polynomials fitted to the data. The curve for the ASME nozzle matches quite well the curve for the matched cubic nozzle. When the data are plotted as a function of Re, the two curves are relatively far apart (this result is not shown). Thus, given S, the near-field base-to-peak intensity is mainly dependent upon D/θ alone. We had formerly remarked (Sreenivasan *et al.* 1989) that the transition to an oscillatory state occurs abruptly with respect to changes in the governing parameters. This is illustrated by the rapid rise in base-to-peak intensity as D/θ increases from its lower limit (see also figure

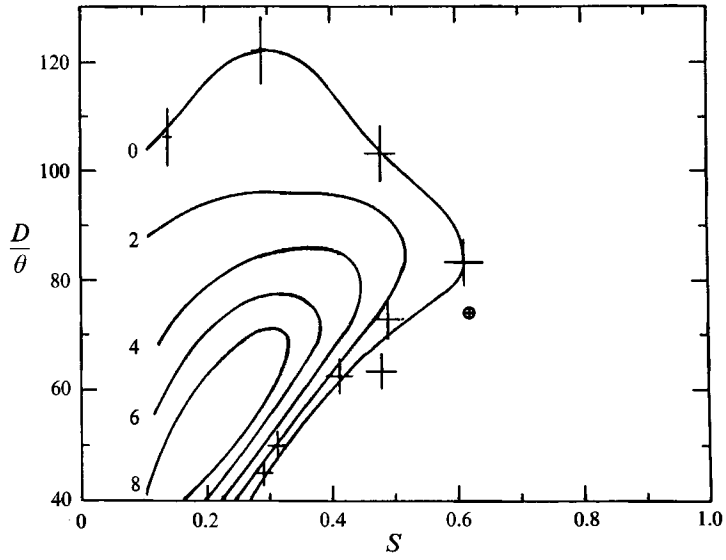

FIGURE 19. Near-field base-to-peak intensity as a function of D/θ and S: contours are labelled with base-to-peak intensity values. The inner contours correspond to larger and larger peak intensities. Error bars denote uncertainty in experimental determination of onset. ⊕, onset in heated air jets (Monkewitz *et al.* 1990).

13). As D/θ nears its upper limit, the base-to-peak intensity varies relatively slowly. This latter aspect is reflected in Sreenivasan *et al.* (1989) by the large error bars used by them.

In summary, we have shown that the non-dimensional frequency of the oscillating mode and its near-field base-to-peak intensity are definite functions of S and D/θ alone. Both these quantities vary significantly with D/θ and do not scale with either D or θ alone. An upper D/θ limit for the oscillating mode has been found for all $S \geqslant 0.14$. This limit is not influenced by either the Mach number or the Reynolds number. Indeed, figure 15 shows that the upper D/θ bound is nearly the same for both nozzles. A lower D/θ limit also exists (except perhaps for $S = 0.14$). Such limits are useful for assessing the accuracy of physical theories (see §7) which predict 'critical values'. They are also important in the practical sense that they help establish the parameter region relevant to the appearance of the oscillating mode.

5.4. *The onset of the oscillatory state*

In this section we study changes in the flow which result from small changes in S near the onset value S_0 for the oscillating mode, for various fixed values of D/θ. Physically, this means that the normalized mean velocity profile at the exit is held fixed as the nozzle fluid density is changed by small increments.

Figure 19 shows the results of systematic measurements of the near-field base-to-peak intensity for the range of ordered pairs $(S, D/\theta)$ relevant to this study. To construct these contours, base-to-peak data were obtained for $S = 0.14$, 0.29, 0.48 and 0.60. At each S, curves were fitted to the data exactly as for figure 18. Data obtained from these curves were used to construct the contours in figure 19. Onset values were further explored by slowly decreasing S at fixed D/θ values of 83, 70, 60 and 50. Error bars are shown for onset values only. The outermost curve marked '0' is the locus of the onset value, S_0, for the oscillating mode and the corresponding D/θ. The region inside this curve (i.e. below and to the left) correspond to inlet flow conditions which

support the oscillating mode. Everywhere outside this curve, the oscillating mode is absent. The S_0, D/θ curve is useful for comparing the onset of the oscillating mode with the predicted onset – or 'critical' – values of S and D/θ associated with absolute instability. Over a range of D/θ values which includes $D/\theta = 83$, critical S values are predicted to lie between 0.66 and 0.72 (Monkewitz & Sohn 1988). Thus, in the vicinity of $D/\theta = 83$ ($S_0 = 0.61$), one might say that there is reasonable correspondence with the theory. On the other hand, consideration of S_0 over a wider range of D/θ values leads to a salient discrepancy: while figure 19 shows that for each $S \leqslant 0.61$ there is an upper bound on the D/θ values for which the oscillating mode can exist, the theory predicts that for all $S \leqslant 0.62$, $\omega_i(k^*(0)) > 0$ even in the limit of $D/\theta \to \infty$ (Monkewitz & Sohn 1986, 1988).

We are interested in the transition to a stable periodic state. Note that the contours in figure 19 are labelled by the base-to-peak intensity. By drawing horizontal cuts through these contours at different constant values of D/θ, one immediately sees that the transition to a stable periodic state brought about by decreasing S can occur in various ways, depending on the choice of D/θ. For example, at $D/\theta = 50$, a small decrease in S below $S_0 \approx 0.31$ is accompanied by a dramatic rise in base-to-peak intensity, whereas at $D/\theta = 83$ base-to-peak intensity varies slowly with S below $S_0 \approx 0.61$.

In order to quantify the effects of D/θ further, the square root of the power spectral density of u' at f_0, u'_{f_0}, is shown in figure 20 non-dimensionalized using U_e, for $D/\theta = 50$, 62.5, and 83. The data are plotted as functions of the normalized density difference $\Delta S = (S_0 - S)/S_0$. The spectra were measured using a hot wire located at $x = 10\theta$, and $r/D = 0.55$ for all three D/θ values. Shadowgraph images for each flow condition revealed no detectable helium present at these locations.

Figure 20 shows that the functional relation between u'_{f_0}/U_e and ΔS is different at different values of D/θ. The uncertainty in ΔS results primarily from the uncertainty in the empirically determined value of S_0. For small ΔS, the data in figure 20 may be fitted to power laws of the form:

$$\left.\begin{aligned} u'_{f_0}/U_e &= a(\Delta S)^n \quad (\Delta S > 0), \\ u'_{f_0}/U_e &= 0 \qquad\quad (\Delta S \leqslant 0), \end{aligned}\right\} \tag{5.1}$$

where the free parameters a and n are determined by the fitting algorithm. For $D/\theta = 50$, $a = 10^{1.5}$ and $n = 1.3$, while for $D/\theta = 62.5$, $a = 10^{1.0}$ and $n = 1.36$. For $D/\theta = 83$, the gradient changes sharply at $\Delta S \approx 0.15$, so that significant error occurs if the power law relation (5.1) is fitted to the data spanning the entire interval $0 \leqslant \Delta S \leqslant 0.76$. If the model (5.1) is applied only to points lying inside the interval $\Delta S \leqslant 0.15$, however, the power-law assumption seems suitable, with $a = 10^{-1.3}$ and $n = 0.55$. It should be mentioned that the measurements were repeated at two other radial locations with the results that the coefficient a becomes smaller for points further away from the jet (and is thus a function of position), but the exponent n was essentially independent of the probe position.

Monkewitz *et al.* (1990) measured the amplitude of near-field pressure fluctuations in a parameter region quite near to the latter truncated range (onset occurred at $D/\theta \approx 74$, $S = 0.62$). A power-law relation provided a good fit when they assumed the power-law exponent $n = 0.5$ for data spanning the interval $\Delta S \leqslant 0.26$. They further noted that Landau's weakly nonlinear stability theory (Landau & Lifshitz 1959) predicts the r.m.s. amplitude of a discrete temporal instability should lie on the parabola $u'^2 \propto \Delta S$ when ΔS is small. Figure 20 shows that, while Landau's theory may apply to the data at $D/\theta = 83$, it fails for $D/\theta = 50$ and 62.5.

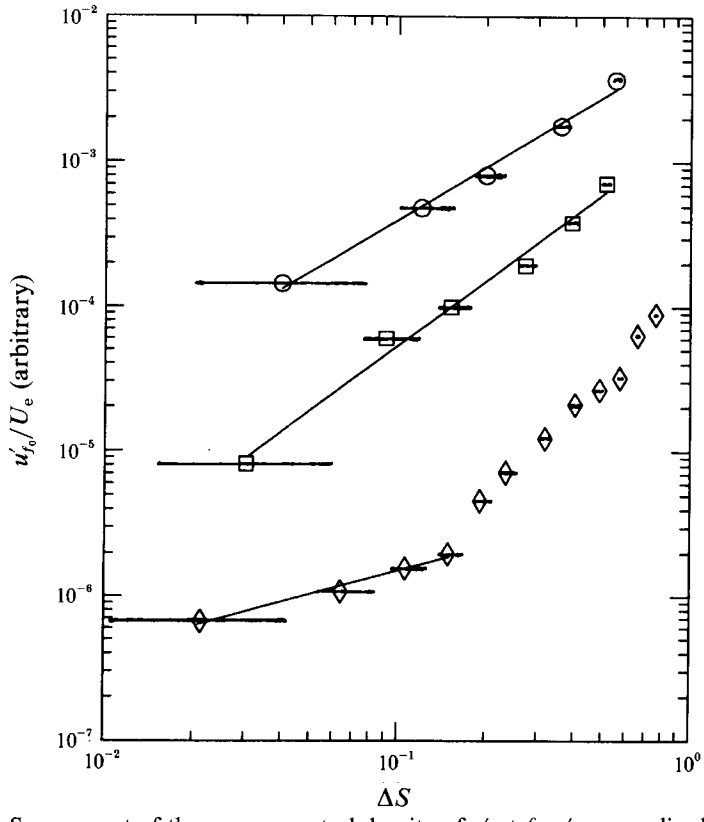

FIGURE 20. Square root of the power spectral density of u' at f_0, u'_{f_0}, normalized by U_e, and plotted as a function of $\Delta S = (S_0 - S)/S_0$ for various D/θ: The power spectrum was measured with respect to an arbitrary reference voltage which was constant for all of the measurements. ◇, $D/\theta = 83$; □, $D/\theta = 62.5$; ○, $D/\theta = 50$. $S = 0.14$; $r/D = 0.55$. The uncertainty in S_0 (see figure 19) is the primary source of uncertainty in ΔS.

This failure is not unexpected. Recall that Landau & Lifshitz (1959) derived the equation beginning with the factorization

$$u'_{f_0}/U_e = A(t; S_0 - S)f(x), \tag{5.2}$$

which assumes that the spatial eigenfunction f is independent of the control parameter S near the critical value S_0. The data of figure 12 (see §4.4) suggest that Landau's assumption concerning $f(x)$ near onset does not apply, say, at $D/\theta = 50$. The large intensities shown in figure 12 for $S = 0.29$ correspond with $\Delta S \approx 0.07$, which may be considered small. Even so, the velocity profiles shown in figure 12 imply that the mean flow divergence is profoundly altered by the onset of the oscillating mode. Recall further from table 1 (§4.2) that for $D/\theta = 50$ and 60, small reductions in S correspond with relatively large reductions in the wave-breaking length. These results suggest that the mean flow in the transition region can be significantly affected by the onset of the oscillating mode, especially at D/θ of the order 50. Figure 20 shows that near onset, the near-field spectral intensity and its gradient are largest at just these D/θ values. One may therefore conclude that for D/θ values of the order 50, the rapid increase in near-field disturbance intensity close to the onset can lead to significant variations in the mean flow structure. If the spatial distribution of fluctuation intensity is related to the structure of the mean flow, it follow that (5.2) should not hold for these D/θ values.

Although there is considerable variation in the character of the onset of the

oscillating mode, one may interpret the occurrence of a stable periodic state in homogeneous round jets as a 'bifurcation' of a nonlinear system from an equilibrium state. Although there are obvious problems with this interpretation, such as defining the equilibrium state, the bifurcation is a supercritical one for flow conditions pertaining to this study. This result is in contrast with the findings of Sreenivasan *et al.* (1989) for a small range of parameters; they used a 4.0 mm nozzle and found that the oscillating mode was *conditionally stable* i.e. that the transition to a stable periodic state should be modelled as a *subcritical bifurcation.* We believe that this difference in behaviour is due to changes in the mean velocity profiles at the nozzle exit; however, because of the small size of that nozzle, we could not measure the velocity profile.

5.5. *Streamwise evolution of the oscillating mode*

In §4, the growth and interaction of large-amplitude vortical structures were examined. We were able to distinguish kinematically between the waves associated with the oscillating mode and waves associated with shear-layer modes usually studied in homogeneous jets. In this section we aim to explore this distinction further by examining their streamwise dependence near the nozzle, where the disturbances are still small. We first establish a method for determining the most spatially amplified mode between any two streamwise locations in the air jet, and then extend it to study heterogeneous jets. For reasons that will be made clear later, this method is most instructive when the oscillating mode is relatively weak. Therefore most of the measurements are obtained at D/θ values near 83, for which it has been shown (see §4.2) that oscillation intensities are small.

Figure 21(*a*) shows power spectra for u' measured using a hot wire located in the shear layer of an air jet where $U/U_e = 0.60$ at streamwise locations $x/\theta = 50$, 100, 200 and 300; $D/\theta = 93$ for this flow. All four spectra are normalized by the maximum spectral amplitude at $x/\theta = 300$. It is evident that the mode at 670 Hz plays a dominant role in the evolution of the shear layer for these conditions. This mode is prominent at $x/\theta = 50$ and grows continually until it dominates the spectrum at $x/\theta = 200$. At $x/\theta = 300$ the subharmonic has become dominant.

We would like to characterize the growth of small disturbances in a region of the jet where nonlinear effects are small. With this intention we focus on the region $x/\theta \leqslant 100$. Figure 21(*b*) shows the ratio of spectral amplitudes at $x/\theta = 100$ to those at $x/\theta = 50$ at corresponding frequencies f. This function simply equals, at any given frequency, the spatial growth rate of disturbances integrated between $x/\theta = 50$ and $x/\theta = 100$. The mode that is most spatially amplified corresponds to the maximum value of this function.

Comparison of the total amplification function (figure 21*b*) with the spectra in figure 21(*a*) reveals that the most energetic mode at $x/\theta = 200$ (670 Hz) is not the most amplified mode in the near field (≈ 860 Hz). The spectra indicate that the mode at 670 Hz becomes dominant owing to the combined effects of its near-field prominence and its subsequent amplification. That the initial velocity-independent spectral distribution of u' could affect the frequency of the most energetic mode further downstream in the shear layer was shown by Cohen & Wygnanski (1987); see also Becker & Massaro (1967) and Gutmark & Ho (1983). The total amplification curve (figure 21*b*) allows one to distinguish between amplification, which varies relatively smoothly with frequency, from the influence of initial field, which varies randomly.

Similar information can be extracted from the total amplification function in heterogeneous jets, as long as the disturbances are sufficiently small. In figure 22, the amplification of shear-layer disturbances between $x/\theta = 25$ and 75 is shown as a

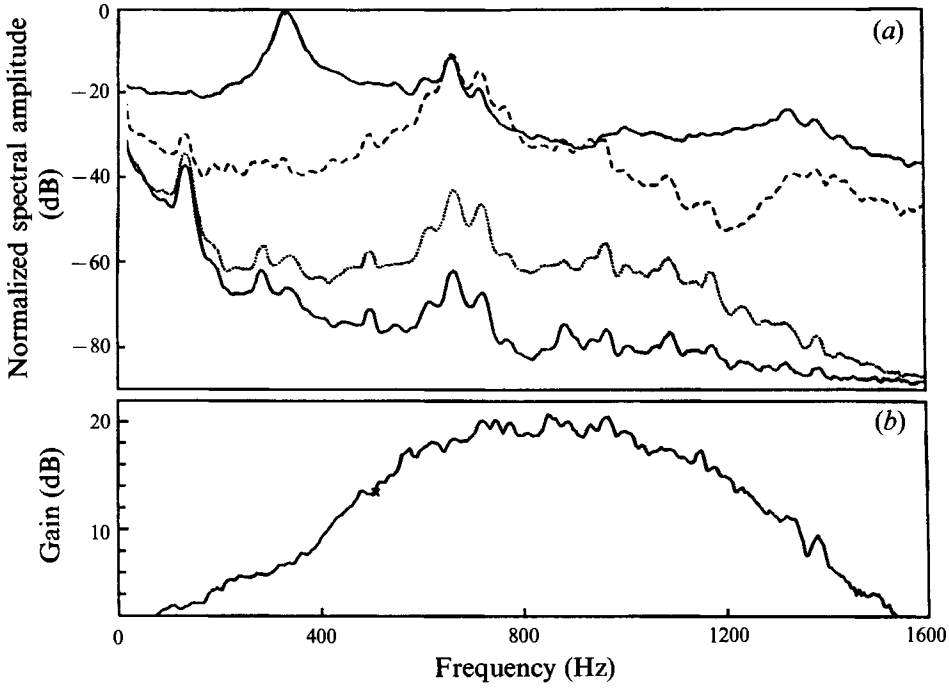

FIGURE 21. (*a*) Normalized power spectra of u' obtained in the shear layer of an air jet at various streamwise locations: ——, $x/\theta = 50$; · · · · ·, $x/\theta = 100$; – – – –, $x/\theta = 200$; ——, $x/\theta = 300$. $S = 1.0$; $U/U_e = 0.6$; $D/\theta = 93$. (*b*) Mode amplification between 50θ and 100θ as a function of frequency using spectra shown in (*a*).

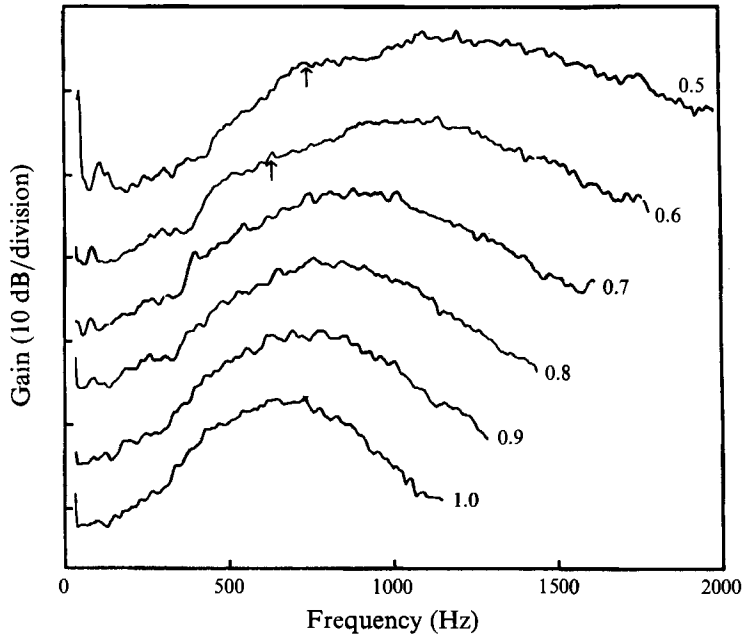

FIGURE 22. Mode amplification between $x/\theta = 25$ and $x/\theta = 75$ as a function of frequency for various values of S. Curves are labelled with S. The gain at each S is determined to within an arbitrary constant factor. Arrows indicate the frequency of the oscillating mode.

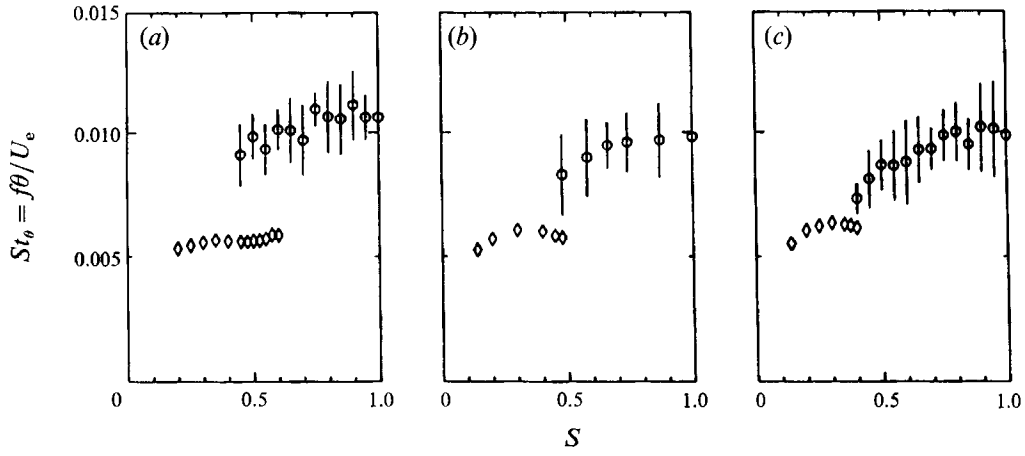

FIGURE 23. Non-dimensional frequency $f\theta/U_e$ plotted as a function of S for (*a*) $D/\theta = 83$; (*b*) $D/\theta = 73$; (*c*) $D/\theta = 62.5$. ◇, oscillating mode; ○, most amplified mode as measured between $x/\theta = 25$ and 75. Errors bars denote measurement uncertainty.

function of frequency for S values ranging from 1.0 to 0.50, for $D/\theta = 83$. (For reasons described in the Appendix, these curves are known only to within an undetermined constant.) Notice that the curves resemble one another in shape, and that the frequency of the most amplified mode varies smoothly with S. This continuity suggests that the underlying physical processes involved in the streamwise amplification of disturbances in homogeneous shear layers are not drastically different from those in the inhomogeneous shear layer for this range of density ratios. This result is substantiated by the general agreement found in §4.2 between the wavelength of regular shear-layer waves and the theoretically predicted value. To our knowledge, this result has not been experimentally confirmed previously (see discussion in Michalke 1984). Regarding the oscillating mode, recall from figure 19 that for $D/\theta = 83$ the jet supports oscillations whenever $S \leqslant 0.61$. The frequency of the oscillating mode for $S = 0.60$ and 0.50 is indicated in figure 22 by an arrow. We note that the frequency of oscillations is distinct from that of the most spatially amplified mode. Evidently, for $D/\theta = 83$ the jet supports both modes simultaneously. We shall shortly see how this observation is consistent with the observed dominance of the oscillating mode.

In figure 23 the non-dimensional frequency of both the oscillating mode and the most spatially amplified mode are plotted as functions of S for $D/\theta = 83$, 73 and 62.5. Notice that the curves for the two modes do not overlap for $D/\theta = 73$ and 62.5. For these D/θ, the oscillating mode is very intense close to the nozzle even for S near S_0. As a result, the harmonics of the oscillating mode grow rapidly in the region $25 \leqslant x/\theta \leqslant 75$, and indeed dominate the amplification curve for $S < S_0$. For all three D/θ, there is no obvious relationship between the frequencies of the most spatially amplified mode and of the oscillating mode. This result could not have been obtained from any scaling argument, simply because no experimental study has been conducted which shows how the most spatially amplified mode varies as a function of either D/θ or S. In fact it is clear from figure 23 that direct measurements are required to show that the frequencies are unrelated.

We note that $f\theta/U_e$ for air jets shown in figure 23 are close to those measured by Michalke (1971), but are some 30% below Drubka & Nagib's (1981) data (= 0.013). The latter authors non-dimensionalized the frequency using θ measured away from the nozzle. Because the momentum thickness increases with x, this procedure yields a

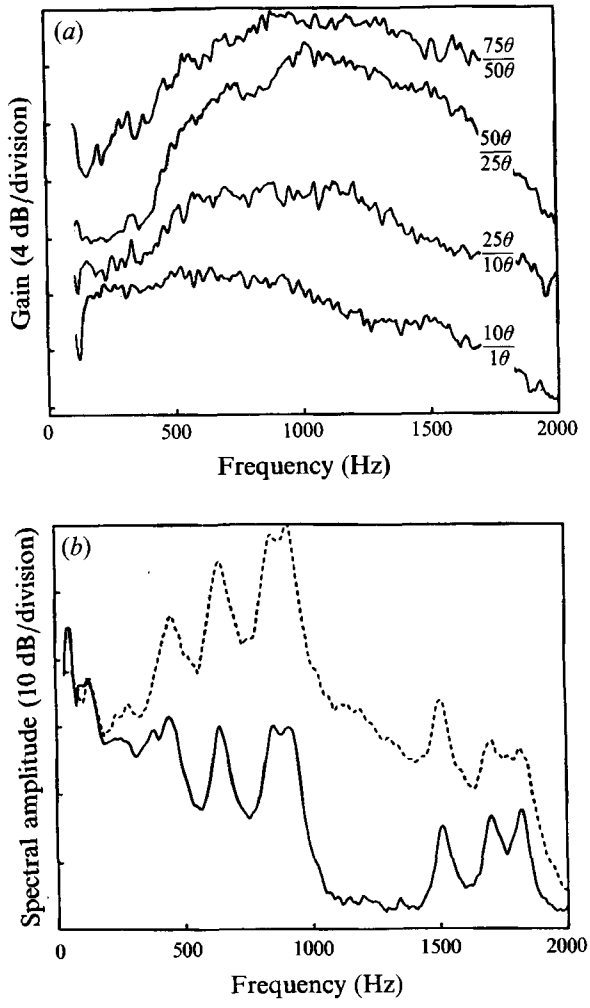

FIGURE 24. (*a*) Mode amplification as a function of frequency: $S = 0.50$; $D/\theta = 83$. Curves are labelled with the appropriate streamwise interval. The gain at each S is determined to within an arbitrary constant factor. (*b*) Power spectra of u' obtained in the shear layer: ——, $x/\theta = 1$; – – – –, $x/\theta = 75$. $S = 0.50$; $D/\theta = 83$. The arbitrary reference for the dB scale differs between the two curves.

higher value for $f\theta/U_e$; Drubka & Nagib indeed noted that θ increased by 40% in the first 80 momentum thicknesses downstream. Regarding the theory, the maximum spatial growth rate is predicted to occur at slightly lower $f\theta/U$ values as S is decreased (Michalke 1984). This agrees qualitatively with the data depicted in figure 23. It should be noted that the absolute value $f\theta/U_e$ corresponding with the spatially most amplified mode was found to be some 30–40% below the predicted value, both for $S = 1.0$ and 0.5. This is reminiscent of the fact that in numerous other studies on naturally excited cold air jets, $f\theta/U_e$ for the most energetic shear layer mode observed was likewise some 30–40% below the predicted value (e.g. Gutmark & Ho (1983).

To understand how the oscillating mode tends to dominate the flow field in spite of the fact that it is not associated with spectacular growth rates, we examine in figure 24(*a*) the streamwise evolution of the oscillating mode between $x/\theta = 1$ and 75 by partitioning the interval into four smaller subintervals, and evaluating the amplification

curves for each of the subintervals. For each subinterval, the total amplification of the oscillating mode (560 Hz) is not sharply distinguished from the amplification at neighbouring frequencies. The net total amplification between $x/\theta = 1$ and 75 may be viewed by comparing the power spectra obtained at the two locations, as seen in figure 24(*b*). Figures 24(*a*, *b*) together show that for $D/\theta = 83$, the large base-to-peak intensity of the oscillating mode is established right at the nozzle.

Our observations, in summary, are that, for $D/\theta = 83$, the base-to-peak intensity measured in the immediate vicinity of the nozzle is generally close in value to that measured at other locations upstream of the wave-breaking point; quite generally, in fact, the oscillating mode is not a consequence of an anomalous spatial growth. In the next section, we examine the effect that acoustic signals and other controlled changes to the environment have on the oscillating mode.

6. Response to acoustic forcing and other changes in the environment

6.1. *Sensitivity to coherent disturbances*

It has been established that the Strouhal number of the oscillating mode is independent of the maximum initial shear-layer disturbance level u'/U_e, even when u'/U_e varies by more than a factor of 2 (see figure 15). We can therefore say that the frequency selection is determined uniquely by the overall flow configuration, and by S and D/θ. Figure 18 (§5.2) shows similarly that the near-field base-to-peak intensity is not systematically affected by u'/U_e over the parameter region of interest. This means that a large component of the oscillation intensity is determined by the overall flow, as distinct from external sources. This appears to be so in spite of the significant random scatter seen in figure 18.

The following experiment is aimed at helping us understand the influence that time-dependent, spatially-coherent disturbances can have on the oscillation intensity. The disturbance is a sinusoidal acoustic signal which is spatially coherent in the sense that the acoustic wavelength is much larger than the spatial scales of the flow: $fD/a_\infty \ll 1$. Spatially coherent disturbances could arise in 'unforced' experiments as well, either from acoustic cavity resonances of the upstream settling chamber, or from uncontrolled far-field acoustic sources.

6.1.1. *Overall response*

In figure 25, the r.m.s. value of the hot-wire signal, E', is plotted as a function of x/θ for different values of the acoustic forcing strength, p'. p' is actually calculated using the voltage which drives the loudspeaker, which is directly proportional to the radiated acoustic pressure. These curves in figure 25 provide only a qualitative comparison of fluctuation intensities at differing streamwise locations, because even close to the nozzle, the mean velocity and the mean helium concentration differ for each x/θ, and so the proportionality constant relating E' and u' changes from place to place.

Figure 25(*a*) shows the response of the heterogeneous jet when forced at a frequency (860 Hz) that is unrelated to the oscillating mode (740 Hz). For the range of forcing amplitudes considered, the 860 Hz mode grows in a roughly exponential fashion until nonlinear damping inhibits further amplification. The growth rate in the near field ($x/\theta \leqslant 50$) appears to be unaffected by the forcing amplitude; the forcing merely augments the spectral intensities in a spatially uniform manner. The maximum intensity attained with downstream distance appears to be nearly independent of the forcing amplitude, except that the maximum is reached closer to the nozzle for larger

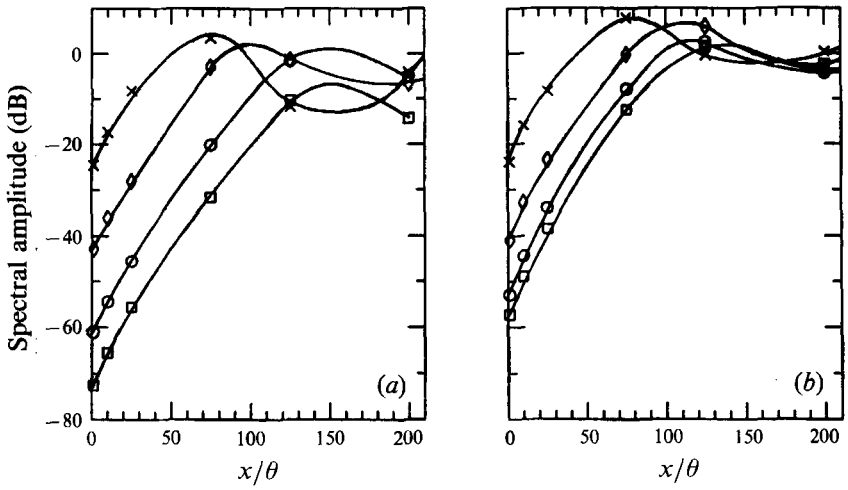

FIGURE 25. The magnitude of the signal from a hot wire located in the shear layer, plotted as a function of x/θ for various acoustic pressure levels p': □, no forcing; ○, 30 dB; ◇, 50 dB; ×, 70 dB. $S = 0.45$; $D/\theta = 83$. (*a*) Pure tone forcing at 860 Hz, and (*b*) pure tone forcing at 740 Hz (oscillating mode).

forcing amplitudes. Acoustically excited shear-layer modes in air jets exhibit these same response characteristics (Frymuth 1966).

Figure 25(*b*) shows that these qualitative results also hold when the same jet is excited at the frequency of the oscillating mode. The two principal differences are: first, the intensity of the oscillating mode in the absence of forcing is significantly greater than the 860 Hz mode; secondly, the fractional increase in intensity induced by the controlled forcing is correspondingly less for the oscillating mode.

Figure 25 helps to explain previous studies in acoustically forced heterogeneous jets. The present authors (Kyle 1986; Sreenivasan *et al.* 1989) found that at a fixed location in the flow, the oscillating mode was essentially insensitive to acoustic forcing, while other shear-layer modes exhibited linear dependence on p' when p' was small. For the present conditions, this behaviour is found at $x/\theta = 100$, where the oscillating mode response is nearly independent of the forcing amplitude (figure 25*b*); whereas, the shear-layer modes, because they are initially less intense, show definite dependence on acoustic forcing when the forcing is small or moderate (figure 25*a*).

6.1.2. *Excited portion of the response*

In order to obtain a more detailed, quantitative picture of the response to external forcing, it is convenient to decompose the velocity field as follows:

$$u' = u'_{\mathrm{N}}(x, r, \text{low-level disturbances}) + u'_{\mathrm{E}}(x, r, p'). \tag{6.1}$$

Here, u' is the measured intensity of velocity fluctuations in the presence of external acoustic forcing. u'_{N} is the response of the jet with no externally applied acoustic forcing; it is dependent upon the partial coordinates, x and r, and possibly upon low-level disturbances arising from within the jet facility and the ambient. u'_{E} is the excited portion of the response, and is dependent upon the spatial coordinates and upon p'. This decomposition is essential for recognizing the behaviour of u'_{E} – which alone is a function of the forcing amplitude – whenever u'_{N} is of comparable magnitude; this situation occurs when the jet is forced at the frequency of the oscillating mode. Note that (6.1) neither requires nor implies that receptivity is a linear process.

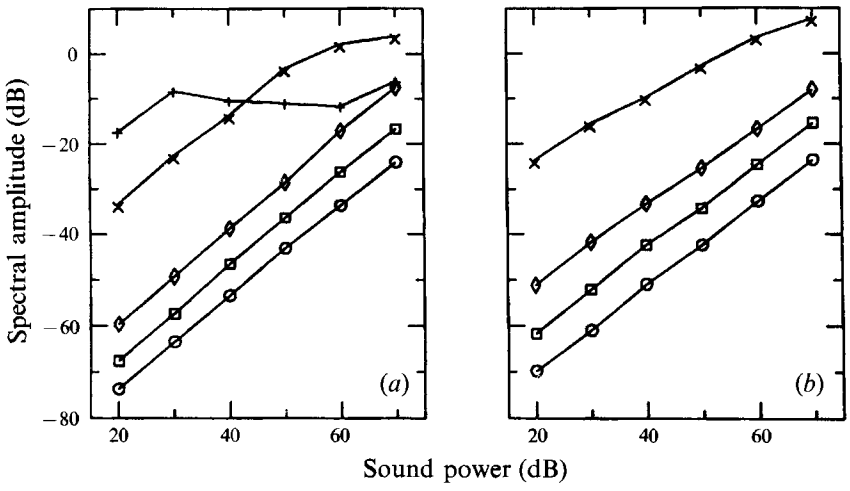

FIGURE 26. Excited portion of the response u_E as a function of p': ○, $x/\theta = 1$; □, $x/\theta = 10$; ◇, $x/\theta = 25$; ×, $x/\theta = 75$; +, $x/\theta = 200$. $S = 0.45$; $D/\theta = 83$. (*a*) Pure tone forcing at 860 Hz, and (*b*) pure tone forcing at 740 Hz (oscillating mode). The arbitrary reference for the dB scale varies from curve to curve.

Figure 26(*a*) shows u_E plotted as a function of p' at various streamwise locations at 860 Hz for the same flow conditions as in figure 25. It is expected that $E' \propto u'$ for data obtained at fixed probe locations very close to the nozzle, say for $x/\theta = 1$, where the acoustically excited disturbances are small enough that they do not significantly affect the mean flow. The data show that for excitation levels spanning approximately two decades, u_E is proportional to the forcing amplitude at $x/\theta = 1$, 10 and 25. It is seen that the linear portion of these three curves are all parallel to one another with slope equal to unity. Hence they must satisfy

$$\log_{10} u_E = \log_{10} p' + G(x), \tag{6.2}$$

where $G(x)$ does not depend upon p'. Letting $G(x) = \log_{10} g(x)$, (6.2) may be rewritten as

$$u_E = p' g(x), \tag{6.3}$$

where $g(x)$ describes the dependence of u_E on x. From (6.3) it is clear that receptivity is indeed a linear phenomenon for heterogeneous flows, just as it is for homogeneous shear flows. To our knowledge, this result has not been shown previously. In fact, (6.3) is a generalization of the results obtained for air jets by Freymuth (1966) who found $g(x) = Be^{\alpha x}$, with B and α dependent upon St_D alone. Although the amplification function $g(x)$ cannot be evaluated in this case, (6.3) shows that growth rate in the near field for the 860 Hz mode is independent of the initial disturbance intensity. This result is reflected in figure 25(*a*), where the amplification curves are all parallel to one another in the near field.

Figure 26(*b*) shows u'_E as a function of p' when the forcing frequency is set equal to the oscillating mode frequency. Note that these conditions are quite far from the onset, as $\Delta S \approx 0.25$. It is seen that u'_E is approximately proportional to p' at $x/\theta = 1$. Furthermore, for these flow conditions, the data suggest that (6.2) and (6.3) obtain with only slight error over a region extending from $x/\theta = 1$ to a location somewhere between $x/\theta = 25$ and $x/\theta = 75$. Thus, background disturbances can affect the evolution of vortical structures associated with the oscillating mode in much the same

way as they do in air jets. Indeed if such disturbances are very strong, figure 25 suggests that they may also affect the wave-breaking length and the overall structure of the mean field in the transition region.

Finally, we recall experimental results presented in Sreenivasan *et al.* (1989) for the case of extremely intense sinusoidal forcing. There, it was shown that the flow can exhibit behaviour that is characteristic of a coupled nonlinear oscillator, in that the oscillatory instability can become entrained or 'locked-in' to the frequency of the forcing.

6.4. *Test for the sensitivity to the turbulence level at the nozzle exit*

We have shown earlier that the frequency of the oscillating mode is independent of weak ambient disturbances. In the following experiment, we examine whether strong, spatially incoherent vortical fluctuations originating upstream of the nozzle have a strong effect on the stability of the oscillating mode (see also Strykowski & Russ 1992).

Two screens of differing mesh sizes were installed separately into the throat of the 13.3 mm nozzle, and the resulting qualitative changes in the power spectrum were observed using a hot wire located on the jet centreline. Although the screens were not fully characterized, the turbulence levels along the centreline in the nozzle plane were measured. The results for $Re = 3380$ were: (*a*) with no screen, $u'/U_e = 0.003$; (*b*) with the small-mesh screen, $u'/U_e = 0.022$; (*c*) with the large-mesh screen, $u'/U_e = 0.055$.

The nozzle fluid was then changed to helium while maintaining the same Re, and the three spectra shown in figure 27 were obtained. With no screen, the fundamental rises 25 dB above the background noise, with prominent harmonics. With the small-mesh screen, the fundamental rose only 20 dB and is somewhat broadened. With the large-mesh screen, the fundamental rose 25 dB above the noise and retained its 'spikiness'; however, its harmonics were attenuated relative to the flow without the screen. Thus, even at moderately high turbulence levels (of the sort not found in respectable jet facilities), the discrete frequency nature of the instability was not quenched. For both screens the frequency decreased. This is not surprising when one considers that the turbulent boundary layer must be thicker than the laminar one, and so by the scaling laws described in § 5, the frequency is expected to decrease.

6.5. *Test for the sensitivity to the ambient environment*

Another experiment was made to test the sensitivity of the oscillating mode to the spatial confinement of the jet. If the jet is surrounded by an open-ended circular container sitting on the nozzle block, the oscillating mode hardly changes in intensity but shows a frequency increase by about 6 or 7% when the container diameter and height are about ten nozzle diameters. When the top of the container is covered by a flat board with a small central hole (diameter on the order of the nozzle diameter), the oscillating mode disappears; this is not surprising because the recirculating flow set up in the container renders, in due course, the density of the ambient gas equal to that of the nozzle gas. Experiments with several geometrical combinations of the container have suggested to us that the oscillating mode disappears only under drastic changes of the environment.

6.6. *Sensitivity to local perturbations*

While the oscillating mode is robust to many types of perturbations, it is quite sensitive to modifications of the mean velocity field. A case in point is its behaviour in the presence of an external body such as a small-diameter pin located at a suitable place inside the flow. This was investigated by Sreenivasan *et al.* (1989) who placed in the centre of the jet perpendicular to the axis a straight pin of a certain diameter and

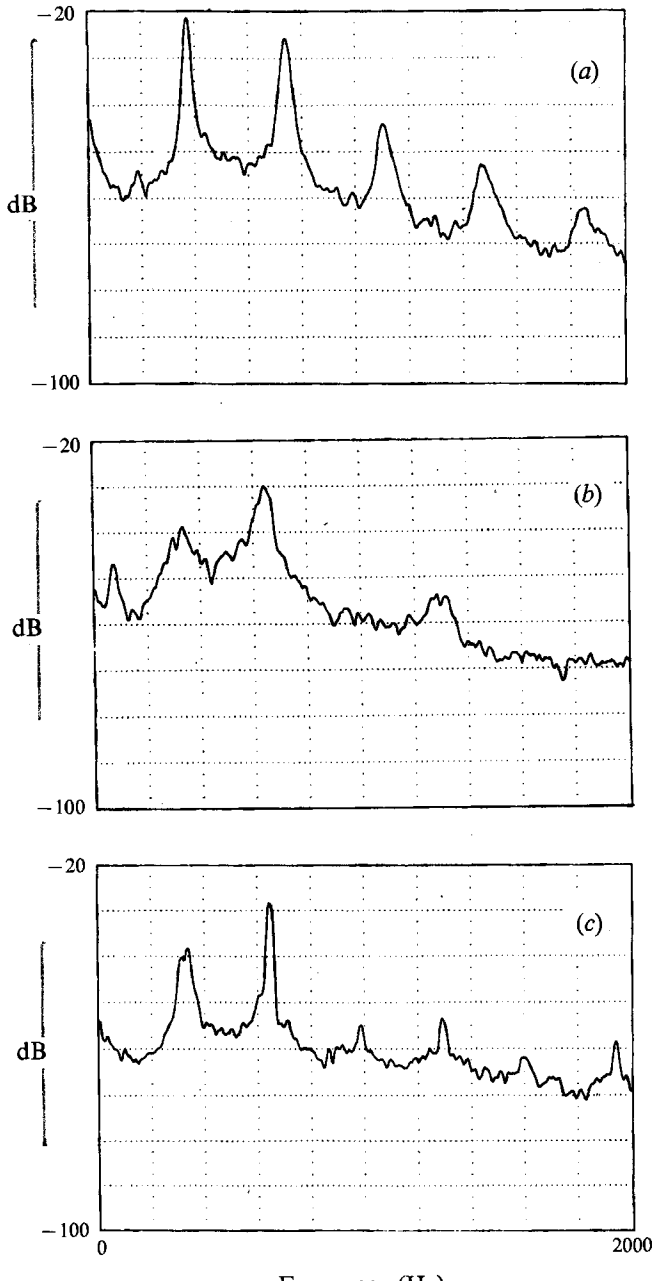

FIGURE 27. Power spectra showing the influence of grid-generated turbulence on the oscillating mode: $S = 0.14$; $D/\theta = 55$; $x/D = 2$; $r = 0$; $D = 13.3$ mm. (*a*) No grid, $u'/U_e = 0.003$; (*b*) finer grid, $u'/U_e = 0.022$; (*c*) coarser grid, $u'/U_e = 0.055$.

monitored the oscillating mode as a function of the pin position along the axis. Typically, the pin diameter was an order of magnitude smaller than the nozzle diameter. They observed that the oscillating mode could be suppressed whenever the pin was located in a certain neighbourhood in the flow. The observation suggests the possibility that the oscillating mode is a consequence of a local instability of the flow

in that neighbourhood, and that it disappear because the pin significantly disrupts the mean flow near where the instability arises (see also Monkewitz *et al.* 1990). It should be noted that perturbations to the mean velocity profile can affect the jet development in isothermal air jets as well (Bradbury & Khadem 1975).

7. Summary and discussion

7.1. *Distinction between various modes*

In heterogeneous jets which do not support the oscillating mode, shear-layer disturbances evolve in an analogous manner to those in constant density jets. We have found that very close to the nozzle, the power spectrum of u' is determined by a combination of the background spectral peaks at the nozzle exit and the spatial amplification rate of shear-layer modes. The latter is a smoothly varying function of the frequency of the disturbance. The maximum of this function is the 'most spatially amplified mode'. The most spatially amplified mode is a smoothly varying function of S. The non-dimensional frequency $f\theta/U_e$ of this mode is in agreement with other experimental studies in air jets. $f\theta/U_e$ decreases with S, as predicted by the spatial stability theory for non-uniform density jets. From films we found that the average value of the wavelength λ/θ is also well-predicted by the theory.

Important changes occur whenever the jet supports the oscillating mode. The structure in the near-field is highly organized both spatially and temporally, and centreline values of u'/U_e can become extraordinarily large. The processes of wave breaking and roll-up formation occur relatively close to the nozzle. The non-dimensional intensity of the oscillating mode and Strouhal number are definite functions of S and D/θ alone, that is they are not systematically affected by background disturbances or by Re within the parameter ranges of this study. The 'most spatially amplified' shear-layer mode also depends smoothly on S and D/θ, but the characteristics $(\lambda/\theta, f\theta/U_e)$ of this mode have been shown to be unrelated to those of the oscillating mode. The base-to-peak intensity of the oscillating mode measured in the immediate vicinity of the nozzle is generally close in value to measurements made further downstream in the near field. Thus, the shear layer acts as a spatial amplifier in the usual way; the oscillating mode does not exhibit an anomalously large spatial growth rate. The initial intensity of the oscillating mode can be influenced by acoustic forcing in a linear fashion, but in a quiet laboratory this component is small relative to the flow-induced portion.

7.2. *Vorticity*

Although we have not measured the vorticity distribution in the presence of the oscillating mode, it is possible to argue that the oscillating mode is associated with highly concentrated vortical structures. The instability of small disturbances in a laminar jet results in the migration of vorticity to form periodic concentrations. In a qualitative sense, the flow field which accompanies such vorticity disturbances is analogous to the nonlinear solutions of the vorticity equation introduced by Stuart (1967). These solutions, which are periodic in one direction and have shear in the other, were used by Stuart to describe the flow patterns in a shear layer with periodic vorticity. The stream function ψ for these solutions is given by

$$\psi = cr + \ln[C\cosh(r) + A\cos(x - ct)], \tag{7.1}$$

where c is the wave speed, and A and C are related by

$$A = (C^2 - 1)^{\frac{1}{2}}. \tag{7.2}$$

The parameter C indicates the degree of concentration of the vorticity: $C = 1$ corresponds to uniform vorticity in the x-direction, while $C \to \infty$ corresponds to a row of point vortices (Lamb 1945). Stuart calculated u'/U_e using (7.1) and (7.2) and found that at every point in the flow, the intensity increases monotonically with C. Note that the area integral of vorticity over any fixed region does not change with C in Stuart's solution; only the distribution is affected. The conclusion is that for a given amount of mean vorticity, the velocity fluctuation intensity can be strongly affected by the degree to which the vorticity disturbance is concentrated. We have measured the r.m.s. velocity u'/U_e along the centreline for two jets with density ratios $S = 1.0$ and $S = 0.29$ but with identical (non-dimensional) mean vorticity distribution at the nozzle exit (§4.4). We found that the jet supporting the oscillating mode ($S = 0.29$) exhibits significantly larger centreline fluctuation intensities (figure 12). This suggests that the vorticity is much more concentrated in the streamwise direction in jets which support the oscillating mode.

Winant & Browand (1974) have proposed a model for the vortex pairing process based on Stuart's solution. Their data show that for a given wave speed, both the initial growth rate of the subharmonic instability and the co-rotating speed of pairing vortices will increase with C. If it is true that the vorticity is more highly concentrated for the oscillating mode, then Winant & Browand's results would suggest that for $S = 0.29$, the pairing process should occur sooner and that the process should be more energetic. We have indeed shown (see table 1) that the pairing generally occurs sooner in jets dominated by the oscillating mode, and that the fluctuation levels reaches abnormally intense values (figure 12) near the location of vortex pairing.

7.3. *Theoretical models*

7.3.1. *Linear theory*

We have not succeeded in experimentally identifying the direct physical cause of the unusual instability arising under certain circumstances in variable-density jets. Various measurements discussed in §§4 and 5 show that a plausible explanation is provided by the linear theory for wave packet growth. Agreement and disparity between theory and experiment will now be reviewed.

If $\omega_i(k^*(0)) > 0$, the theory shows that in a streamwise homogeneous system, any spatially localized disturbance will, as time increases, lead to an increasingly monochromatic response, as observed. In fact, for $S = 0.50$ there is a reasonable correspondence between the predicted and observed values of $f\theta/U_e$, within a limited range of D/θ values around 80. In this same range of D/θ, approximate correspondence has been found between the predicted critical value of $S(= 0.72)$ and the observed onset value $S_o(= 0.61)$.

On the other hand, as D/θ increases much above about 80, the correspondence with the theory breaks down. In contradiction to the theory, S_o rapidly takes smaller values with increasing D/θ (figure 19). For large enough values of D/θ the oscillating mode vanishes, even though the theory predicts that for all $S \leqslant 0.62$, $\omega_i(k^*(0)) > 0$ even in the limit of $\theta \to 0$ (Monkewitz & Sohn 1986, 1988). A complete validation of any linear stability theory might comprise a matching of velocity data with computed eigenfunctions and eigenvalues, and a matching of any predicted critical parameter values with their experimentally determined onset values. By these standards, the correspondence between the oscillating mode and the spatio-temporal theory summarized in §1 would seem quite scant.

Even the somewhat limited correspondence found in §§4 and 5 between the linear theory and experiment may seem surprising because: (*a*) the instability theory assumes

homogeneity in the streamwise direction, whereas the flow in the near field is strongly inhomogeneous, and (*b*) the oscillating mode is so intense that linear mechanisms can be called into question without much thought. As regards (*a*), we have shown that the oscillating mode is global in the sense that the separate processes involved in laminar–turbulent transition occur in a globally organized fashion. On the other hand, its initiation may be related to the local spatio–temporal instability of a certain profile in the near field. Some support for this for this conjecture comes from Chomaz, Huerre & Redekopp (1988) who have shown that it is possible to construct a one-dimensional linear system which exhibits just this behaviour. They have shown that if a certain coefficient of the linearized Ginzburg–Landau equation is allowed to vary spatially, then within the context of that system, the existence of temporally growing modes of the form $\phi(x)\,\mathrm{e}^{\mathrm{i}\omega t}$ always requires that $\omega_{\mathrm{i}}(k^*(0)) > 0$ for some spatial interval (see the review by Huerre & Monkewitz 1990). Concerning (*b*), a common experience is that the frequency of instability between the linear and nonlinear stages does not vary much. We stress that, although the linear theory might help in understanding the behaviour of the instability, large-amplitude motions play an essential role in sustaining the stable periodic state overall.

7.3.2. *Nonlinear theory*

Raghu & Monkewitz (1991) have pointed out that considerable physical insight might be obtained from studying the temporal growth of the oscillating mode. They have tried to show that the oscillatory disturbance field in a heated air jet can be modelled as a 'global temporal mode', that is,

$$u'(x,t) = A(t)f(x), \tag{7.3}$$

and that this mode obeys the Landau equation. Because of the similarity between the two flows, such a conclusion would also be appropriate to the heterogeneous flows considered here. Unfortunately, their results are inconclusive in that they obtained data at only a single streamwise location and provide no information as to whether the factorization (7.3) is valid. Moreover, our examination of onset for a wide range of flow conditions (§5.4) indicates that the spatial distribution of fluctuation intensity can itself be strongly amplitude-dependent near onset. For such behaviour the factorization (7.3) is inappropriate. Yet, the 'bifurcation' appears to be of the supercritical type for jets produced in many laboratory facilities. (For an exception under certain circumstances, see Sreenivasan *et al.* 1989.) In further pursuit of this line of inquiry, we propose that transient response simultaneously measured at different streamwise locations would be very valuable. At least under flow conditions with slow transient growth, one might learn more about the incipient stages of the oscillating mode.

We thank Professors Edward Bolton and Boa-Teh Chu for useful discussions. The work was financially supported by a grant from the Air Force of Scientific Research.

Appendix. Interpreting hot-wire spectra of small disturbance in laminar heterogeneous shear layers

While one is primarily interested in measuring the power spectral density of u' in the shear-layer region, a single hot wire cannot be used in regions of variable density where the mass fraction of helium c fluctuates. This is because the hot-wire voltage E is affected by both fields:

$$E(t;x,r) = E(c(t;x,r), U(t;x,r)). \tag{A 1}$$

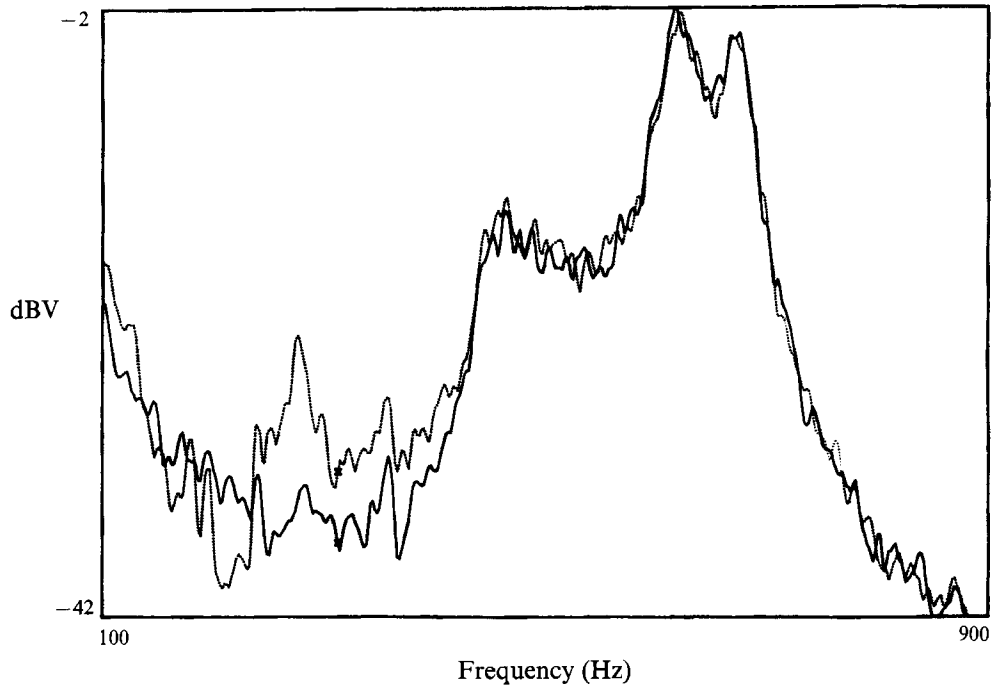

FIGURE 28. Power spectra of u' obtained at different radial locations in the shear layer region: $S = 1.00$; $D/\theta = 83$; $x/\theta = 75$; ——, potential core; – – – –, $r = \frac{1}{2}D + 5\theta$. The arbitrary reference for the dB scale varies for the two curves.

Instead, the power spectral density of u' has been obtained using a hot wire placed within the 'potential core' region, where both the mean velocity and the mean helium concentration are uniformly distributed in the radial direction. Because c can only decrease owing to mixing, it follows that concentration fluctuations are altogether absent in the potential core. For each of the flows discussed in this Appendix, the existence of this region has been confirmed. In each example, the hot wire was placed very near to where either U or c (or both) is just beginning to decrease with r, i.e. near the 'inner edge' of the shear layer. At this location the hot wire responds only to the velocity fluctuations associated with shear-layer disturbances, which are presumed to be strong along the inner edge of the shear layer (see Freymuth 1966).

Flow uniformity within the potential core, as well as the location of the inner edge of the shear layer, was confirmed in each case as follows. As the hot wire is moved radially outward from the centreline by small increments δr, the mean voltage changes according to:

$$E(r+\delta r) - E(r) = \frac{\partial E}{\partial U}\frac{\partial U}{\partial r}(\delta r) + \frac{\partial E}{\partial c}\frac{\partial c}{\partial r}(\delta r). \tag{A 2}$$

The partial derivatives $\partial E/\partial U$ and $\partial E/\partial c$ have been measured directly by placing the hot wire at the centre of the nozzle exit and separately varying U and c for several different conditions. It was found that $\partial E/\partial U$, $\partial E/\partial c > 0$, while $(\partial E/\partial U)/(\partial E/\partial c)$ is of order unity (see also Way & Libby 1971). Because $\partial U/\partial r$, $\partial c/\partial r < 0$ the mean voltage will always decrease with r. Thus, the radial extent of the potential core can be unambiguously determined.

Unfortunately, it is not convenient to rely upon measurements obtained in the potential core because the presence of the probe itself can alter the evolution of shear-

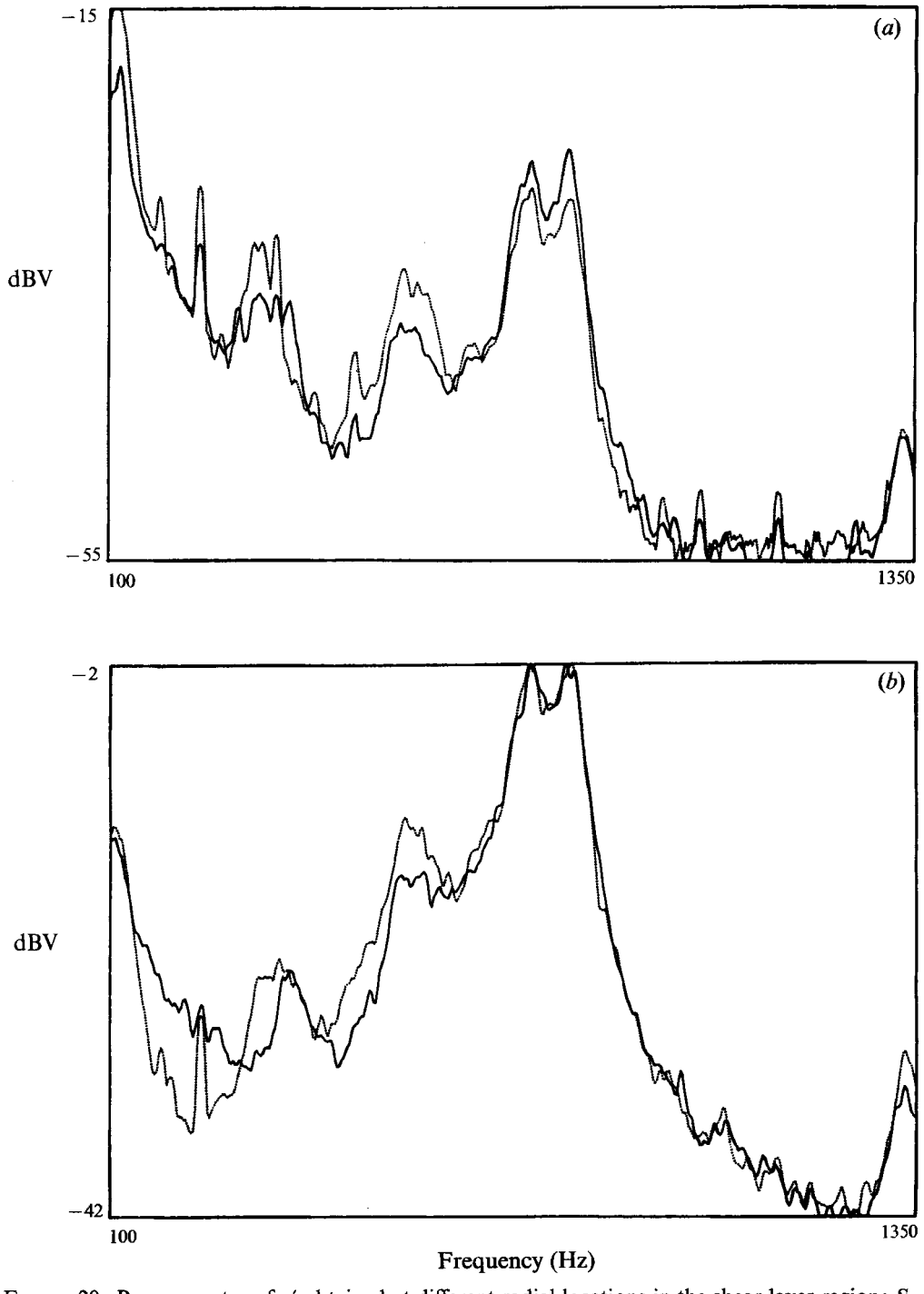

FIGURE 29. Power spectra of u' obtained at different radial locations in the shear layer region: $S = 0.70$; $D/\theta = 83$; ----, potential core; ——, $r = \frac{1}{2}D + 5\theta$. (*a*) $x/\theta = 25$; (*b*) $x/\theta = 75$. The arbitrary reference for the dB scale varies for the two curves.

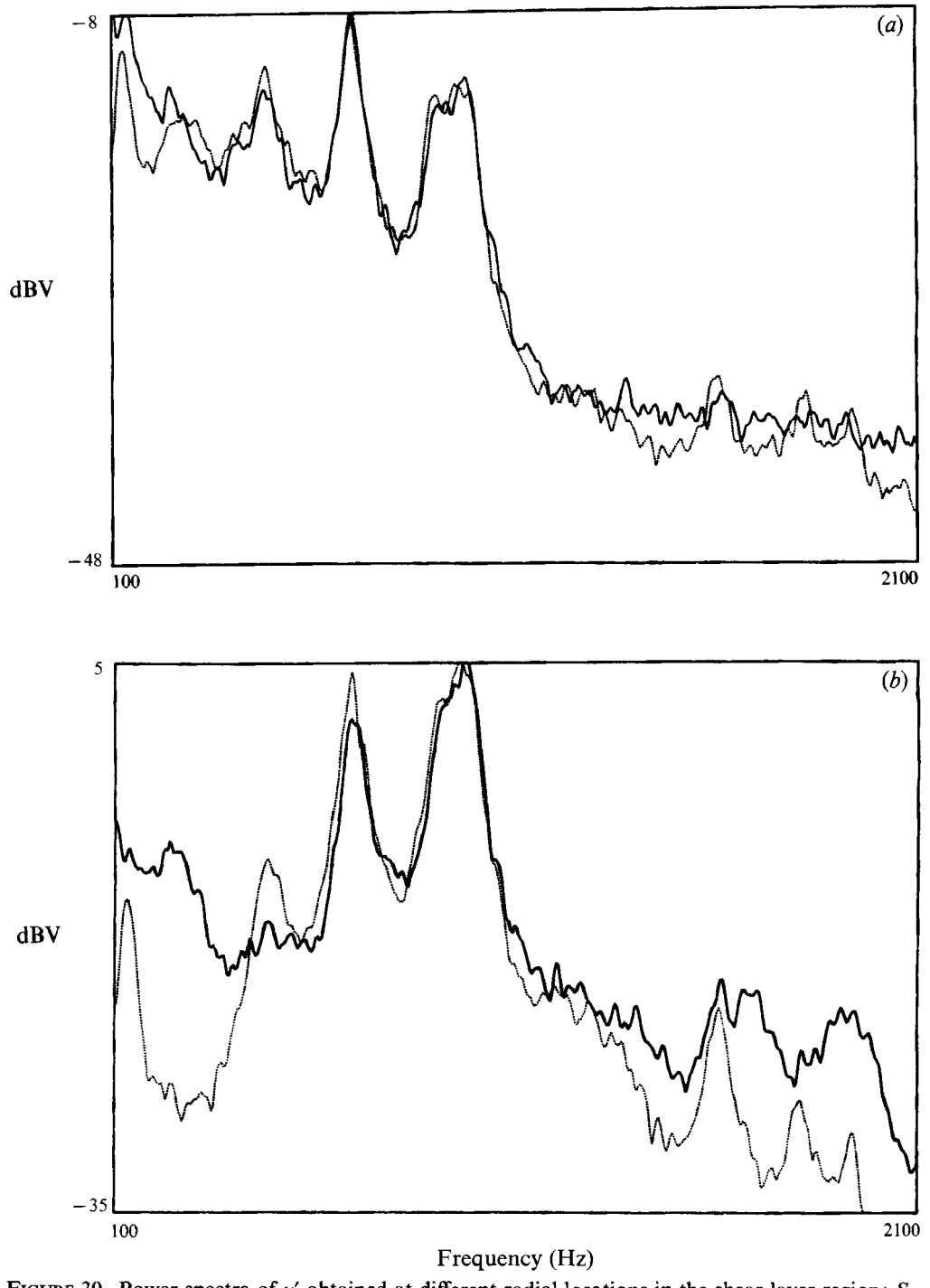

FIGURE 30. Power spectra of u' obtained at different radial locations in the shear layer region: $S = 0.50$; $D/\theta = 83$; – – –, potential core; ——, $r = \frac{1}{2}D + 5\theta$. (*a*) $x/\theta = 25$; (*b*) $x/\theta = 75$. The arbitrary reference for the dB scale varies for the two curves.

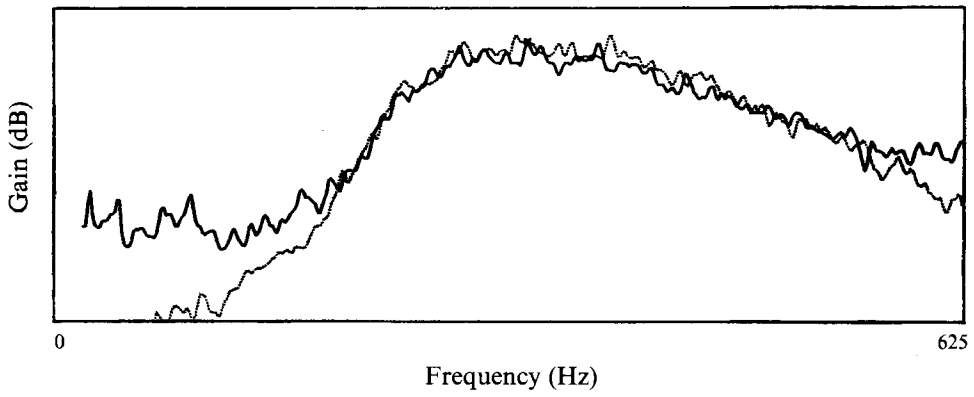

FIGURE 31. Mode amplification between $x/\theta = 25$ and $x/\theta = 75$ as a function of frequency for two different radial locations: $S = 0.60$; $D/\theta = 62.5$; ----, potential core; ——, $r = \frac{1}{2}D + 5\theta$. The gain at each r is determined to within an arbitrary constant factor.

layer disturbances (Hussain & Zaman 1978; Sreenivasan *et al.* 1989). We have therefore measured the spectrum near the outer edge of the shear layer at $r = \frac{1}{2}D + 5\theta$ and exploited the result, discussed below, that in regions near the nozzle where disturbances are small, the power spectral density function obtained at $r = \frac{1}{2}D + 5\theta$ is approximately the same as the power spectrum of u' obtained in the potential core, except for a constant factor which is independent of the frequency.

Figure 28 shows power spectra of u' obtained in an air jet within the potential core ($r = \frac{1}{2}D - 10\theta$) and near the outer edge of the shear layer ($r = \frac{1}{2}D + 5\theta$) at $x/\theta = 75$. The spectra have been multiplied by arbitrary constants selected to show the similarity in the form of the curve. It is seen that the spectra are very similar, except at the lowest frequencies. Measurements in air jets obtained at different streamwise locations $x/\theta < 75$ and for differing D/θ all yield similar results. Figure 29 shows power spectra for $S = 0.70$ at $x = 25\theta$ and 75θ. Again the spectra obtained within the potential core and at $r = \frac{1}{2}D + 5\theta$ are approximately the same except for a constant normalizing factor. Figure 30(*a*) shows that this similarity can extend even to jets which support the oscillating mode, so long as measurements are made close to the nozzle. In figure 30(*b*), the similarity has degraded somewhat, presumably owing to large-amplitude effects. Note that for each potential core measurement, possible effects associated with the intruding probe were monitored using a second hot wire located well outside the shear layer. No intrusion effects were observed for the examples shown in figures 28–30.

During the course of this study, spectra obtained at $r = \frac{1}{2}D + 5\theta$ are used for calculating the following measures: (i) base-to-peak intensity measured in the immediate vicinity of the nozzle ($x/D = 0.10$). Whenever probe intrusion is not a factor, this measure is found to be roughly independent of r (see figure 30*a*). (ii) Most spatially amplified mode (§4.4). Figure 29 suggests that the functional relation between spatial amplification rate and frequency should be approximately independent of the radial position, except for a constant factor that is independent of frequency. More particularly, the maximum of the spatial amplification curve (§5.5) should be independent of radial position. This is confirmed in figure 31 for $S = 0.60$ and $D/\theta = 62.5$. Again, the spectra are seen to differ most in form at the lowest frequencies. (iii) Frequency of the oscillating mode. This measure is actually a constant for all points in the transitional flow.

REFERENCES

ABRAMOVICH, G. N., YAKOVLEVSKY, O. V., SMIRNOVA, A. N. & KRASHENINNIKOV, S. Y. 1969 An investigation of the turbulent jets of different gases in a general stream. *Acta Astron.* **14**, 229–240.

BEAN, H. S. (ed.) 1971 *Fluid Meters: Their Theory and Application.* ASME.

BECKER, H. A. & MASSARO, T. A. 1968 Vortex evolution in a round jet. *J. Fluid Mech.* **31**, 435–448.

BERS, A. 1983 Space–time evolution of plasma instabilities – absolute and convective. In *Handbook of Plasma Physics* (ed. M. N. Rosenbluth & R. Z. Sagdeev), vol. 1, pp. 451–517. North-Holland.

BRADBURY, L. J. S. & KHADEM, A. H. 1975 The distortion of jets by tabs. *J. Fluid Mech.* **70**, 801–813.

BRADSHAW, P. 1966 The effect of initial conditions on the development of a free shear layer. *J. Fluid Mech.* **26**, 225–236.

BRIGGS, R. J. 1964 *Electron Stream Interaction with Plasmas.* Research Monograph no. 29. MIT Press.

BROWAND, F. K. & LAUFER, J. 1975 The role of large scale structures in the initial development of circular jets. In *Turbulence in Liquids* (ed. J. L. Zakin & G. K. Patterson), pp. 333–344. Princeton, NJ: Science Press.

BROWN, G. L. & ROSHKO, A. 1974 On density effects in turbulent mixing layers. *J. Fluid Mech.* **64**, 775–816.

CHAN, Y. Y. & LEONG, R. K. 1973 Discrete acoustic radiation generated by jet instability. *CASI Trans.* **6** (2), 65–72.

CHOMAZ, J. M., HUERRE, P. & REDEKOPP, L. G. 1988 Bifurcations to local and global modes in spatially developing flows. *Phys. Rev. Lett.* **60**, 25–28.

CHRISS, D. E. 1968 Experimental study of the turbulent mixing of subsonic axisymmetric gas streams. *AEDC-TR-68-133* (available through NTIS).

COHEN, J. & WYGNANSKI, I. 1987 The evolution of instabilities in the axisymmetric jet. Part 1. The linear growth of disturbances near the nozzle. *J. Fluid Mech.* **176**, 191–219.

CORRSIN, S. T. & UBEROI, M. S. 1949 Experiments on the flow and heat transfer in a heated turbulent jet. *NACA Tech. Note* 1865.

CROW, S. C. & CHAMPAGNE, F. H. 1971 Orderly structure in jet turbulence. *J. Fluid Mech.* **48**, 547.

CRIGHTON, D. G. 1975 Basic principles of aerodynamic noise generation. *Prog. Aero. Sci.* **16**, 31–96.

DAVIES, P. O. A. L. & BAXTER, D. R. J. 1977 *Transition in Free Shear Layers* (ed. H. Fiedler). Lecture Notes in Physics, pp. 125–135. Springer.

DRUBKA, R. E. & NAGIB, H. M. 1981 *Fluids and Heat Transfer Report R81-2.* Department of Mechanical and Aerospace Engineering, Illinois Institute of Technology.

FREYMUTH, P. 1966 On transition in a separated laminar boundary layer. *J. Fluid Mech.* **25**, 683–704.

GASTER, M. 1962 A note on the relation between temporally-increasing and spatially-increasing disturbances in hydrodynamic stability. *J. Fluid Mech.* **14**, 222–224.

GASTER, M. 1965 On the generation of spatially growing waves in a boundary layer. *J. Fluid Mech.* **22**, 433–441.

GASTER, M. 1968*a* Growth of disturbances in both space and time. *Phys. Fluids* **11**, 723–727.

GASTER, M. 1968*b* The development of three-dimensional wave packets in a boundary layer. *J. Fluid Mech.* **32**, 173–184.

GASTER, M. & DAVEY, A. 1968 The development of three-dimensional wave packets in unbounded parallel flows. *J. Fluid Mech.* **32**, 801–808.

GEANKOPLIS, C. J. 1972 *Mass Transport Phenomena.* Holt, Rinehart and Winston.

GUTMARK, E. & HO, C. M. 1983 Preferred modes and the spreading rates of jets. *Phys. Fluids* **26**, 2932–2938.

HO, C. M. & HUANG, L. S. 1982 Subharmonics and vortex merging in mixing layers. *J. Fluid Mech.* **119**, 443–473.

HOCH, R. G., DUPONCHEL, J. P., COCKING, B. J. & BRYCE, W. D. 1973 Studies of the influence of density on jet noise. *J. Sound Vib.* **28**, 649–668.

HUERRE, P. & MONKEWITZ, P. 1985 Absolute and convective instabilities in free shear layers. *J. Fluid Mech.* **159**, 151–168.

HUERRE, P. & MONKEWITZ, P. 1990 Local and global instabilities in spatially developing flows. *Ann. Rev. Fluid Mech.* **22**, 473–537.

HUSSAIN, A. K. M. F. & RAMJEE, V. 1976 Effects of the axisymmetric contraction shape on incompressible turbulent flow. *Trans. ASME* I: *J. Fluids Engng* **98**, 58–69.

HUSSAIN, A. K. M. F. & ZAMAN, K. B. M. Q. 1978 The free shear layer tone phenomenon and probe interference. *J. Fluid Mech.* **87**, 349–381.

HUSSAIN, A. K. M. F. & ZEDAN, M. F. 1978 Effects of the initial condition on the axisymmetric free shear layer: Effects of the initial momentum thickness. *Phys. Fluids* **21**, 1100–1111.

KIBENS, V. 1980 Discrete noise spectrum generated by an acoustically excited jet. *AIAA J.* **18**, 434–441.

KOCH, W. 1985 Local instability characteristics and frequency determination of self-excited wake flows. *J. Sound Vib.* **99**, 53–83.

KOTSOVINOS, N. E. 1975 A study of the entrainment and turbulence in a plane buoyant jet. W. M. Keck Lab. Hydraul. Water Res. *Caltech Rep.* KH-R-32.

KYLE, D. 1986 Absolute instability in variable density jets. *Dept. Mech. Engng Rep.* 86FM6. Yale University.

KYLE, D. 1988 LIF images of He/N_2 jets. *Dept. Mech. Engng Rep.* FM88DK1. Yale University.

KYLE, D. 1991 The instability and breakdown of a round variable-density jet. PhD thesis, Department of Mechanical Engineering, Yale University.

KYLE, D. & SREENIVASAN, K. R. 1988 Discrete frequency phenomena in variable density round jets. *Bull. Am. Phys. Soc.* **33**, 2232 (abstract only).

KYLE, D. & SREENIVASAN, K. R. 1989 Stability properties of He/air jets. *Proc. ASME/ASCE Forum on Chaotic Flows*, LaJolla, CA (in press).

LAMB, L. 1945 *Hydrodynamics*. Dover.

LANDAU, L. D. & LIFSHITZ, E. M. 1959 *Fluid Mechanics. 6. Course of Theoretical Physics.* Pergamon.

LANDIS, F. & SHAPIRO, A. H. 1951 *The Turbulent Mixing of Co-axial Gas Jets.* Heat Transfer and Fluid Mechanics Institute. Stanford University Press, California.

LIEPMANN, D. 1991 Streamwise vorticity and entrainment in the near field of a round jet. *Phys. Fluids* A **3**, 1175–1185.

LONG, M. B., FOURGUETTE, D. C., ESCODA, M. C. & LAYNE, C. B. 1983 Instantaneous Ramanography of a turbulent diffusion flame. *Optics Lett.* **8** (5), 244–246.

MASLOWE, S. A. & KELLY, R. E. 1971 Inviscid instability of an unbounded heterogeneous shear layer. *J. Fluid Mech.* **48**, 405–415.

MICHALKE, A. 1971 Instabilitat eines Kompressiblen Runden Freistrahls unter Berucksichtigung des Einflusses der Strahlgrenzschichtdicke. *Z. Flugwiss.* **19**, 319–328.

MICHALKE, A. 1984 Survey on jet instability theory. *Prog. Aerospace Sci.* **21**, 159–199.

MONKEWITZ, P. A., BECHERT, D. W., BARSIKOW, B. & LEHMANN, B. 1990 Self-excited oscillations and mixing in a heated round jet. *J. Fluid Mech.* **213**, 611–639.

MONKEWITZ, P. A., LEHMANN, B. T., BARSIKOW, B. & BECHERT, D. W. 1989 The spreading of self-excited hot jets by side jets. *Phys. Fluids* **7**, 446–448.

MONKEWITZ, P. A. & SOHN, P. A. 1986 Absolute instability in hot jets and their control. *AIAA paper* 86-1882.

MONKEWITZ, P. A. & SOHN, P. A. 1988 Absolute instability in hot jets. *AIAA J.* **26**, 911–916.

MORKOVIN, M. V. & PARANJAPE, S. V. 1971 On acoustic excitation of shear layers. *Z. Flugwiss.* **19**, 328–335.

MORRIS, P. J. 1976 The spatial viscous instability of axisymmetric jets. *J. Fluid Mech.* **77**, 511–529.

PAVITHRAN, S. & REDEKOPP, L. G. 1989 The absolute-convective transition in subsonic mixing layers. *Phys. Fluids* A **1**, 1736–1739.

PRASAD, R. R. & SREENIVASAN, K. R. 1990 Quantitative three-dimensional imaging and the structure of passive scalar fields in fully turbulent flows. *J. Fluid Mech.* **216**, 1–34.

RAGHU, S. & MONKEWITZ, P. A. 1991 The bifurcation of a hot round jet to limit-cycle oscillations. *Phy. Fluids* A **3**, 501–503.

RAYLEIGH, LORD 1894 *Theory of Sound*, vol. 1. Macmillan.

SAROHIA, V. & MASSIER, P. F. 1977 Experimental results of large-scale structures in jet flows and their relation to jet noise production. *AIAA J.* **16**, 831–835.

SFORZA, P. M. & MON, R. F. 1978 Mass, momentum, and energy transport in turbulent free jets. *Intl J. Heat Mass Transfer* **21**, 371–384.

SMITH, D. J. & JOHANNESEN, N. H. 1986 The effects of density on subsonic jet noise. *IUTAM Symp. on Aero- and Hydro- Acoustics, Lyons.* Springer.

SREENIVASAN, K. R., RAGHU, S. & KYLE, D. 1989 Absolute instability in variable density jets. *Exps Fluids* 7, 309–317.

STEIN, G. D. 1969 Design of a multipurpose wind tunnel. *Rev. Sci. Instrum.* **40**, 1058–1061.

STRYKOWSKI, P. J. & NICCUM, D. L. 1991 The stability of countercurrent mixing layers in circular jets. *J. Fluid Mech.* **227**, 309–343.

STRYKOWSKI, P. J. & RUSS, S. 1992 The effect of boundary layer turbulence on mixing in heated jets. *Phys. Fluids* **A4**, 865–868.

STRYKOWSKI, P. J. & SREENIVASAN, K. R. 1990 On the formation and suppression of vortex 'shedding' at low Reynolds numbers. *J. Fluid Mech.* **218**, 71–107.

STUART, J. T. 1967 On finite amplitude oscillations in laminar mixing layers. *J. Fluid Mech.* **29**, 417–440.

STURROCK, P. A. 1958 Kinematics of growing waves. *Phys. Rev.* **112**, 1488–1503.

SUBBARAO, E. R. 1987 An experimental investigation of the effects of Reynolds number and Richardson number on the structure of a co-flowing buoyant jet. PhD thesis, Department of Aeronautics and Astronautics, Stanford University, Palo Alto, USA.

TOMBACH, I. H. 1969 Velocity measurement with a new probe in inhomogeneous turbulent jets. PhD thesis, California Institute of Technology.

WAY, J. & LIBBY, P. A. 1971 Application of hot-wire anemometry and digital techniques to measurements in a turbulent helium jet. *AIAA J.* **9**, 1567–1573.

WILKE, C. R. 1950 *J. Chem. Phys.* **18**, 517–519.

WILLE, R. 1963 Beitrage zur Phanomenologie der Freistrahlen. *Z. Flugwiss.* **11**, 222–223.

WINANT, C. D. & BROWAND, F. K. 1974 Vortex pairing: the mechanism of turbulent mixing-layer growth at moderate Reynolds number. *J. Fluid Mech.* **63**, 237–255.

YULE, A. J. 1978 Large-scale structure in the mixing layer of a round jet. *J. Fluid Mech.* **89**, 413–432.